Title

Modern water/rock reactions in Oman hyperalkaline peridotite aquifers and implications for microbial habitability

Authors

Miller, Hannah M
Matter, Jürg M
Kelemen, Peter
et al.

Publication Date

2016-04-01

DOI

10.1016/j.gca.2016.01.033

Peer reviewed

Modern water/rock reactions in Oman hyperalkaline peridotite aquifers and implications for microbial habitability

Author links open overlay panelHannah M.Miller[a]Jürg M.Matter[bc]PeterKelemen[c]Eric T.Ellison[a]Mark E.Conrad[d]NoahFierer[ef]TylerRuchala[g]MasakoTominaga[g]Alexis S.Templeton[a]
Show more

https://doi.org/10.1016/j.gca.2016.01.033Get rights and content

Abstract

The Samail ophiolite in Oman is undergoing modern hydration and carbonation of peridotiteand may host a deep subsurface biosphere. Previous investigations of hyperalkaline fluids in Oman have focused on fluids released at surface seeps, which quickly lose their reducing character and precipitate carbonates upon contact with the O_2/CO_2-rich atmosphere. In this work, geochemical analysis of rocks and fluids from the subsurface provides new insights into the operative reactions in serpentinizing aquifers. Serpentinite rock and hyperalkaline fluids (pH > 10), which exhibit millimolar concentrations of Ca^{2+}, H_2 and CH_4, as well as variable sulfate and nitrate, were accessed from wells situated in mantle peridotite near Ibra and studied to investigate their aqueous geochemistry, gas concentrations, isotopic signatures, mineralogy, Fe speciation and microbial community composition.
The bulk mineralogy of drill cuttings is dominated by olivine, pyroxene, brucite, serpentineand magnetite. At depth, Fe-bearing brucite is commonly intermixed with serpentine, whereas near the surface, olivine and brucite are lost and increased magnetite and serpentine is detected. Micro-Raman spectroscopy reveals at least two distinct generations of serpentine present in drill cuttings recovered from several depths from two wells. Fe K-edge X-ray absorption near-edge spectroscopy (XANES) analysis of the lizardite shows a strong tetrahedral Fe coordination, suggesting a mixture of both Fe(II) and Fe(III) in the serpentine. Magnetite veins are also closely associated with this second generation serpentine, and 2–10 μm magnetite grains overprint all minerals in the drill cuttings. Thus we propose that the dissolved H_2 that accumulates in the subsurface hyperalkaline fluids was evolved through low temperature oxidation and hydration of relict olivine, as well as destabilization of pre-existing brucite present in the partially serpentinized dunites and harzburgites. In particular, we hypothesize that Fe-bearing brucite is currently reacting

with dissolved silica in the aquifer fluids to generate late-stage magnetite, additional serpentine and dissolved H_2.

Dissolved CH_4 in the fluids exhibits the most isotopically heavy carbon in CH_4 reported in the literature thus far. The CH_4 may have formed through abiotic reduction of dissolved CO_2 or through biogenic pathways under extreme carbon limitation.

The methane isotopic composition may have also been modified by significant methane oxidation. 16S rRNA sequencing of DNA recovered from filtered hyperalkaline well fluids reveals an abundance of *Meiothermus*, *Thermodesulfovibrionaceae* (sulfate-reducers) and *Clostridia* (fermenters). The fluids also contain candidate phyla OP1 and OD1, as well as *Methanobacterium*(methanogen) and *Methylococcus* sp. (methanotroph). The composition of these microbial communities suggests that low-temperature hydrogen and methane generation, coupled with the presence of electron acceptors such as nitrate and sulfate, sustains subsurface microbial life within the Oman ophiolite.

- **Previous** article in issue
- **Next** article in issue

1. Introduction

The Samail ophiolite in the Sultanate of Oman, the largest and best exposed ophiolite sequence on Earth, is well-suited to the study of low temperature serpentinization, which is the aqueous alteration of ultramafic rocks. Over 15,000 km^3 of peridotite is currently undergoing low temperature hydration and oxidation (Barnes et al., 1978, Neal and Stanger, 1983, Neal and Stanger, 1985, Clark and Fontes, 1990, Kelemen and Matter, 2008, Kelemen et al., 2011, Paukert et al., 2012, Streit et al., 2012). Modern serpentinization is inferred from the distribution of hyperalkaline seeps that release hyperalkaline fluids rich in H_2 and CH_4, and poor in dissolved inorganic and organic carbon. However, the water/rock reaction pathways giving rise to H_2 and methane formation at near-surface temperatures are not known. Moreover, no studies have yet explored whether the active hydrogeochemical system hosts a subsurface biosphere.

In Oman, the mantle peridotite consists of olivine, orthopyroxene, and serpentine, with trace amounts of calcic pyroxene, chromite, and Fe-oxides (Hanghøj et al., 2010). The mantle peridotite is 30–70% serpentinized (Boudier et al., 2010) and variably carbonated. Some serpentinization occurred during hydrothermal circulation when the ophiolite was situated at an oceanic spreading ridge, some during thrust emplacement of the ophiolite over pelagic and continental margin sediments, some during late

Cretaceous sub-aerial weathering and a subsequent marine transgression, and some during ongoing water/rock reactions (Hanghøj et al., 2010, Kelemen et al., 2011). The proportions and spatial distribution of serpentine and other secondary minerals formed during these different events are unclear. Completely unaltered peridotite is not observed in outcrop in Oman, but the least altered samples are found in deep canyons, whereas the most serpentinized outcrops are in areas of low relief (Kelemen et al., 2011). The peridotite also undergoes carbonation reactions as evidenced by modern carbonate vein and terrace dates (Clark and Fontes, 1990, Kelemen and Matter, 2008, Mervine et al., 2014) which indicate temperatures of formation from 30 to 60 °C (Kelemen et al., 2011, Streit et al., 2012).

An active hydrological system drives present-day serpentinization and other alteration processes occurring in the subsurface. Groundwater circulation in the peridotite aquifer is controlled by fissure and fracture hydraulic conductivity. Near-surface fissures (perhaps extending to ~50 m depth) accommodate most of the groundwater flow with a hydraulic conductivity of 10^{-7} m/s (Dewandel et al., 2005). The origins of this shallow, hydraulically active zone are not clear, but are probably due to meteoric weathering. The peridotite aquifer contains a network of fractures that began to develop when the ophiolite was hydrothermally altered at the mid-ocean ridge, ~95 million years ago during the Middle Cretaceous (Coleman, 1981). The fractures in the peridotite host serpentine and carbonate veins (Dewandel et al., 2005). Hyperalkaline surface seeps generally discharge at the contactbetween the mantle and overlying crustal rocks, and along the basal thrust plane of the ophiolite sequence. They release high pH fluids (>11) rich in Ca^{2+}, OH^-, H_2, and CH_4. The surrounding mineralogy is dominated by carbonates that precipitated when the carbon deprived fluids mixed with atmospheric CO_2 (Kelemen and Matter, 2008, Kelemen et al., 2011, Paukert et al., 2012, Chavagnac et al., 2013a, Chavagnac et al., 2013b).

The origin of dissolved H_2 and CH_4 in Oman are enigmatic. Currently, there is no evidence for modern hydrothermal activity at temperature greater than 200 °C of water/rock reactions in the peridotite aquifer, which would correspond to a depth of ~8 km based on a geothermal gradient of 25 °C/km. Although serpentinization processes have been extensively studied at temperatures >120 °C, the mineral assemblages and alteration processes leading to formation of dissolved H_2 and CH_4 during serpentinization at lower temperatures are poorly constrained. Serpentinization leads to the evolution of hydrogen through hydration and the oxidation of reduced iron species found in olivine and pyroxenes. For typical mantle olivine with molar Mg/(Mg + Fe) = 0.9, a simplified reaction above 200 °C might be:

(1)Mg1.8Fe0.2SiO4+1.37H2O=0.5Mg3Si2O5OH4+0.3MgOH2+0.067Fe3O4+0.067H2
(e.g. Eq. (1); Frost, 1985, McCollom and Bach, 2009). Such water/rock reactions produce fluids rich in H_2. These fluids also commonly contain abundant dissolved CH_4, which may form abiogenically as the result of Fischer–Tropsch Type or Sabatier reactions (Horita and Berndt, 1999, Etiope et al., 2013), or biologically via methanogenesis (Balch et al., 1979, Sleep et al., 2004).

Hydrogen generation during serpentinization has been modeled from 8 to 400 °C (McCollom and Bach, 2009, Okland et al., 2012, Klein et al., 2013a). Experimentally produced H_2 has been generated from 0 to 100 °C (Stevens and McKinley, 1995, Stevens and McKinley, 2000, Anderson et al., 1998, Neubeck et al., 2011, Okland et al., 2012, Mayhew et al., 2013) Comparisons of model and experimental results often yield conflicting results, perhaps because of assumptions included in models. For example, McCollom and Bach (2009) utilize reaction path models to simulate water-rock reactions and resulting mineral assemblages, but they are constrained by the lack of existing thermodynamic data for Mg:Fe solid solutions, the incorporation of Fe(III) into secondary silicates, and the lack of data on mineral compositions that form at low temperature. Also, models assume the reactions have reached equilibrium, and it is unlikely that low-temperature laboratory experiments are fully equilibrated. Thus, detailed analysis of field samples from low-temperature serpentinizing environments is required to ground-truth modeling efforts.

There is also a lack of data on the detection or characterization of microorganisms in Oman's hyperalkaline aquifers. The high concentrations of H_2 and CH_4 in the hyperalkaline fluids provide electron donors that could be utilized by subsurface chemolithoautotrophic life, which could contribute to carbon cycling in the subsurface (Stevens and McKinley, 1995, Sleep et al., 2004, Nealson et al., 2005, Mayhew et al., 2013, Klein et al., 2015). The search for microbial life in other serpentinizing environments has primarily been focused on sequencing the 16S rRNA gene from easily accessible surface springs as windows into the subsurface (Neal and Stanger, 1983, Abrajano et al., 1990, Bruni et al., 2002, Meyer-Dombard et al., 2015, Woycheese et al., 2015), although recent work by Postec et al. (2015)isolated DNA from carbonate chimneys from a low-temperature hydrothermal field. However, all these studies were limited to surface samples collected in oxygenated environments, which allows aerobic organisms to flourish. It is unclear if the microbes inhabiting the surface seeps are similar to those active in the anaerobic subsurface.

This study was designed to assess low temperature serpentinization processes in a peridotite aquifer in Oman and to determine what types of microbial life are hosted in

the subsurface. We sampled hyperalkaline, H_2-, CH_4-rich fluids from 10 to 300 m depth in peridotite and studied their geochemistry, gas concentrations and isotopic signatures. We integrated these data with mineralogical and spectroscopic analysis of mineral chips recovered from depth within two peridotite wells to elucidate the oxidation state, mineralogy, and extent of serpentinization of the rocks in contact with deep subsurface fluids. Magnetic hysteresis analyses on downhole bulk rock samples augment these geochemical and mineralogical analyses by providing the distribution of different rock magnetic propertieswithin drilled sections, thereby suggesting possible zonation in the serpentinization process. Geochemical data were complemented by high throughput 16S rRNA sequencing of DNA recovered from the well fluids to identify microbial organisms present in the fluid. These data provide the first insights into the modern water/rock reactions in a hyperalkaline Oman aquifer, and the potential coupling between geochemical and microbiological processes during low-temperature serpentinization.

2. Methods

2.1. Field methods

The Ministry of Water Resources of the Sultanate of Oman drilled numerous wells into peridotite (~300 m deep) to investigate water resources for the region. Water samples and drill cuttings were obtained from wells NSHQ14 and NSHQ04 in a peridotite plain in the Samail ophiolite, Oman (Fig. 1). NSHQ04 is near a north/south trending fault, with gabbro to the west and mixed dunite and gabbro lenses cut by pyroxenite dikes to the east. NSHQ14 is several kilometers from the crust-mantle boundary; the surrounding rocks are mainly harzburgite with meter-scale dunite bands.

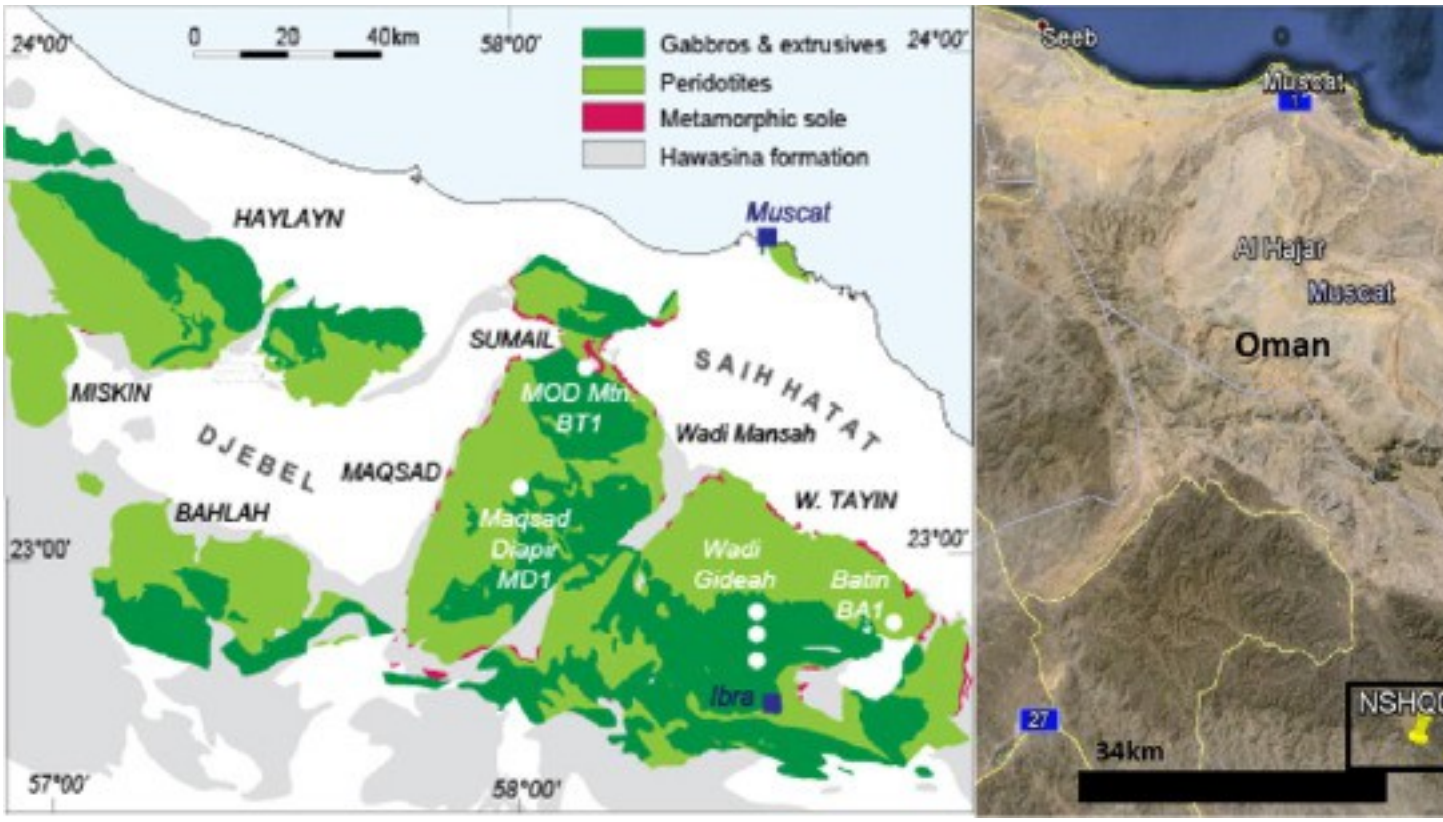

1. Download high-res image (317KB)
2. Download full-size image

Fig. 1. NSHQ04 is located at UTM coordinate 675491 Easting, 2529716 Northing using the WGS-94 datum. NSHQ14 is located at 670975 Easting, 2531692 Northing. The top right picture shows the distribution of the ophiolite in Oman, and the wells are situated in the light green peridotite near the circle labeled Batin (geologic map courtesy of Oman drilling program website). (For interpretation of the references to color in this figure legend, the reader is referred to the web version of this article.)

In January 2014, a shallow submersible pump was used to collect water from 18 m depth in both NSHQ04 and NSHQ14, and a stainless steel bailer was used to collect water from 260 m in well NSHQ14. Water samples containing dissolved gases were collected in sterile syringes and injected into N_2-purged vials and later used for headspace gas analysis. The vials were acid washed, autoclaved and baked at 400 °C in a muffle furnace prior to field work. Samples for ICP-MS analysis were filtered with 0.2 μm Millipore filters and acidified in the field with concentrated nitric acid to ~pH 2. The fluid pH, temperature, and conductivity were measured with a conductivity meter (YSI Model#85/10) while pH was measured with a Mettler-Toledo SevenGo2 pH meter calibrated with reference standards of pH 12.46, 10.01, and 7.

Fluids (~5–10 L) from the wells were pumped and filtered through 0.2 μm Sterivex inline filters to recover biomass for DNA extraction. Filters were transported frozen in liquid nitrogen and stored in a −70 °C freezer until extraction.
We also obtained drill cuttings (rock chips recovered during drilling) of the wells from 262, 140, 70, and 17 m depth at NSHQ14 and from 303, 180, and 120 m depth at well NSHQ04. These were mounted in epoxy and prepared as 30 μm thick polished thin sections for analysis.

2.2. Laboratory methods

Major cations (Na^+, Fe^{2+}, Mg^{2+}, Ca^{2+}, K^+), SiO_2, and trace elements (Ni, As, Se, Cu, Cd, Zn Co, Cr) were analyzed on field-acidified and filtered well waters using Inductively Coupled Plasma-Mass Spectrometry (ICP-MS) on a ThermoScientific X Series 2.
Major anions (F^-, Cl^-, Br^-, NO_3^-, PO_4^{3-}, SO_4^{2-}) were analyzed using Ion Chromatography (IC) on a Dionex IC25 with an IonPac column and a 9 mM sodium carbonate eluent. Water samples were collected in acid-washed, autoclaved, and ashed organic free vials and sent to NASA Ames Research Center to measure low weight molecular organic acids on a Shimadzu Prominence LC20AT high-performance liquid chromatograph (HPLC) equipped with a SPD-M20A photodiodearray detector and a flow rate of 1 mL per minute.
Drill cuttings were powdered with a mortar and pestle and then X-ray diffraction (XRD) data were obtained using CuKα radiation (λ = 1.5418 Å) in the range 15–65° 2θ using a Bruker D2 Phaser operated at 30 kV and 10 mA. A Lynxeye 1D detector with a step size of 0.02° and collection time of 1 s per step were employed. The XRD spectra were semi-quantitatively fit using the Bruker DiffracEva program and results were compared to the RRUFF database (Downs, 2006).
To determine H_2 and CH_4 concentrations (detection limit of 10 ppm and analytical error of 5%) in the gases exsolved from the well fluids, we used a SRI 8610C gas chromatograph (GC) with a 2 m by 1 mm ID micropacked ShinCarbon ST column with N_2 as the carrier gas. 0.5 mL of gas was sampled from the headspace of serum vials sealed with blue rubber stoppers and was injected into a sampling port on the GC. H_2 was measured with a thermal conductivity detector (TCD), and a flame ionization detector (FID) was concurrently used to measure CH_4.
Stable isotope analyses were conducted at the Center for Isotope Geochemistry at the Lawrence Berkeley National Laboratory. The isotopic compositions of H_2 and CH_4 were analyzed using a Thermo Scientific GC Trace Gas Ultra system connected to a Thermo Scientific Delta V Plus Mass Spectrometer (IRMS). Gas samples were injected into a 6-

port valve (the loop size varied from 5 L to 250 L depending on the concentration of the analyte in the sample) bypassing the inlet of the GC. After flushing with at least 3 times the volume of the loop, the sample was injected into the GC where the gases were separated chromatographically on an HP-molesieve fused silica capillary column (30 m × 0.320 mm). For H_2, after the samples went through the GC, they were passed through a combustionfurnace at room temperature and then into the IRMS. Reproducibility of these analyses is ±2.5‰ (1σ), as determined by repeated analyses of a laboratory gas standard. Carbon isotope ratios of CH_4 were analyzed using the same system with the combustion furnace (a capillary ceramic tube loaded with Ni, Cu, and Pt wires) set at 1030 °C where the CH_4 was converted to CO_2. Produced water was removed, and the carbon isotope ratio of the resulting CO_2 was measured in the IRMS. The reproducibility of these analyses is ±0.2‰. For hydrogen isotopes of CH_4, the sample was passed through a pyrolysis furnace at 1450 °C and the resulting H_2 gas measured with the IRMS. The reproducibility of these analyses is ±5‰.

Samples with 10–100 micrograms calcite were reacted with 100% H_3PO_4 at 90 °C and then used for both carbon and oxygen isotope analyses ($\delta^{13}C$ and $\delta^{18}O$), which were determined using a GV IsoPrime mass spectrometer with Dual-Inlet and MultiCarb systems in the Center for Stable Isotope Biogeochemistry (CSIB) at Department of Integrative Biology, University of California at Berkeley. Several replicates of one international standard NBS19, and two lab standards $CaCO_3$-I & II were measured along with samples for each run. The overall external analytical precision is about ±0.05‰ for $\delta^{13}C$ and about ±0.07‰ for $\delta^{18}O$.

The isotopic compositions of the water samples were measured using CIG's Los Gatos Research Liquid Water Isotope Analyzer (LWIA). 1 ml of each sample was loaded into 2 ml vials. Using an auto sampler, each sample was injected into the LWIA 8 times where the data for the first 3 injections were discarded and the data for the remaining 5 injections averaged to give the raw isotope values. The data were then compared to a series of 3 standards bracketing the expected isotopic values of the samples analyzed and run multiple times throughout the run. The reproducibility of these analyses based on repeated analyses of the standards is better than ±1‰ for δD and ±0.2‰ for $\delta^{18}O$.

2.3. Microscale analytical techniques

Synchrotron-based hard X-ray measurements of Fe K-edge micro-X-ray absorption near edge spectra (μXANES) were conducted at Beamline 2-3 at the Stanford Synchrotron Radiation Lightsource (SSRL). The incident energy was selected with a Si (1 1 1) double crystal monochromator with the SPEAR accelerator ring

containing ~150–200 mA at 3.0 GeV. The beam was focused to approximately 2 by 2 μm using Kirkpatrick Baez mirrors. Data were collected at the Fe K-edge using a Fe^0 foil calibration of 7112 eV with a single-element Vortex detector capable of reading several million counts per second.

Fe K-edge mapping was conducted at 8 energies (7123, 7126, 7128, 7129, 7130, 7131, 7133 keV) chosen to maximize the differences in normalized intensity between representative XANES (Mayhew et al., 2011, Mayhew et al., 2013). These data were coupled with an 11 keV map of trace element distribution to identify unique areas in the sample. Principle Components Analysis (PCA) on these multiple energy XRF maps were used to identify the location of unique Fe species in the map area using Sam's Microprobe Analysis Kit (SMAK). We then collected representative μXANES spectra from those spots and employed PCA to identify key end member μXANES spectrum that represent the unique chemical forms of Fe in each sample. Finally, multiple-energy maps were fit with the fluorescence intensities of each end member μXANES spectra to show the distribution of Fe-bearing minerals in complex reacted and unreacted samples.

XANES were normalized with Sam's Interface for XAS Package (SIXPACK). XANES spectra were collected from a range of 6882–7152 eV. To qualitatively determine Fe speciation and mineralogy, spectra were fit from 7110 to 7150 eV using least squares fitting of Fe model compounds (in SIXPACK) calibrated using the first inflection of a Fe^0 foil at 7112 eV (Mayhew et al., 2011). We also collected the pre-edge (7108–7118 eV) region with a step size of 0.1 eV and dwell time of 3 s and analyzed the pre-edge employing protocols by Wilke et al. (2001) and Andreani et al. (2013) to determine the ratio of Fe^{2+}/Fe^{3+} in the various generations of serpentine.

Beamline 4-1 at SSRL was used to collect bulk Fe K-edge spectra for seven powdered well chip samples. A Si (220) $\phi = 0$ monochromator was used and X-ray absorption spectra(XAS) were collected on a Lytle detector. A Fe^0 foil standard was used and calibrated to 7112 eV. Duplicate spectra were collected and averaged for XANES scanning from a range of 6882–7082 eV with a step size of 10 points, then from 7092 to 7520 with a 0.35 step size.

Quantum Design MPMS Superconducting Quantum Interface Device (SQUID) magnetometer with the magnetic moment resolution of 10^{-8} emu at Department of Physics and Astronomy at Michigan State University was used to analyze bulk rock powder samples to determine magnetic hysteresis parameters. A total of 7 samples with various weights (40–259 mg) are measured over the range of ±5 T at 300 K.

Micro-Raman spectra and hyperspectral maps for well rock chip samples were collected using a Horiba LabRAM HR Evolution Raman spectrometer equipped with a 532 nm frequency-doubled Nd:YAG laser (Laser Quantum, Torus 532 + mpc3000) coupled to an Olympus BXFM optical microscope. The laser beam was focused through a 50× objective lens, yielding a spatial resolution of ~2 μm. A 600 lines/mm grating and adjustable confocal pinhole (100–200 μm) was used to give a spectral resolution full width at half maximum (FWHM) of 4.5–8.4 cm^{-1}. Spectra were collected from 20 to 1200 cm^{-1} using a Si-based CCD detector (1024 × 256 pixels). The spectrometer was calibrated using the 520 cm^{-1}Raman peak of Si daily prior to analysis. Spectral data were corrected for instrumental artifacts and baseline-subtracted using a polynomial fitting algorithm in LabSpec 6 (Horiba Scientific). For the Raman microspectroscopy analyses, the drill cuttings from each depth in NSHQ14 and NSHQ04 were analyzed by generating hyperspectral maps of representative areas in the thin sections, using Multivariate Curve Resolution-Alternating Least Squares (MCR-ALS) and non-negativity constraints on scores and loadings to determine the main spectral components present, then collecting spot Raman spectra to verify the components, and fitting the hyperspectral data set with the end member spectra to generate component maps. Quantitative chemical analysis of serpentine was performed using the electron microprobelaboratory at the University of Colorado at Boulder on the JEOL JXA-8600 equipped with 4 wavelength-dispersive spectrometers, and a PGT energy-dispersive spectrometer. Spot analyses of polished thin sections were performed at a current of 10 nA, accelerating voltageof 15 keV, and beam diameter of 10 μm to avoid destroying the hydrated serpentine sample to analyze the major element compositions of Si, Al, Mg, Na, Ca, Cr, K, Fe, Mn, and Ti, using natural standards.
TGA measurements were taken in a NETZSCH STA 449 F1 Jupiter. Between 60 and 110 mg of sample in an alumina crucible and a blank alumina crucible were heated in Argonup to 1000 °C at a ramp rate of 10 Kelvin per minute. The crucibles were then held at 1000 °C for one hour, at which point data collection stopped and the furnace cooled. The derivatives of the data were determined using NETZSCH Proteus.

2.4. 16S rRNA sequencing

The microbial analyses were conducted as described previously (Bowers et al., 2013, Emerson et al., 2015). DNA was extracted from one quarter of each of the filter samples using the MoBio PowerSoil kit. The V4–V5 region of the 16S rRNA gene was PCR amplified in triplicate reactions using the 515f/806r primer pair. The primers contained the appropriate Illumina adapters and the reverse primer contains a 12-bp

error-correcting barcode unique to each sample. The triplicate reactions were composited, amplicon concentrations were determined using the PicoGreen dsDNA assay, and the amplicons from all samples were pooled together in equimolar concentrations. Sequencing was conducted on an Illumina MiSeq at the University of Colorado Genomics Core Facility following the 2 × 250 bp paired-end protocol. Quality filtering of reads and processing of the reads was conducted as described in Barberán et al. (2015). After demultiplexing, reads were quality filtered at an equivalent sequencing depth (6000 reads per sample) and clustered into phylotypes using the UPARSE pipeline (Edgar, 2013). Reads were assigned to phylotypes at the ⩾97% sequence similarity threshold and phylotype taxonomy was determined using the RDP classifier with a confidence threshold of 0.5 (Wang et al., 2007) trained on the Greengenes 13_8 database (McDonald et al., 2012). Multivariate statistical analysis was performed in R, a software environment for statistical computing and graphics (R Development Core Team, 2008).

3. Results

3.1. Aqueous geochemistry of wells

Fluids were collected from two wells drilled into peridotite, NSHQ14 (up to a depth of 260 m) and NSHQ04 (up to a depth of 50 m, below which the well is collapsed). Minimum concentrations of dissolved H_2 and CH_4 were determined by GC. For NSHQ14 at 262 m, some gas was lost from the fluids during the transfer from the bailer sampler to gas-tightvials due to rapid exsolution. The calculated dissolved H_2 concentrations range from 0.18 to 0.67 mM H_2, and the methane concentrations range from 0.17 to 1.44 mM (Table 1).

Table 1. Major and minor elements in wells along with pH, temperature, and conductivity. Oman hyperalkaline spring data is from Paukert et al. (2012) sampling Type II surface waters. Oxidation-reduction potential (ORP) data is from sampling the wells in 2012. Gas concentrations were determined by measuring the headspace of anaerobic vials purged with N_2 filled with site water.

	NSHQ04 18 m	NSHQ14 18 m	NSHQ14 260 m	Misbit – Oman hyperalkaline spring	Detection limit (μM)
pH	10.6	11.1	11.5	11.2	–
Temperature (°C)	33.3	34.3	31.5	31.6	–
Conductivity (μS/m)	2386	2430	4300	1640	–
ORP (mV)	−103.4 (70 m)	−31.6	−597.3	–	–

	NSHQ04 18 m	NSHQ14 18 m	NSHQ14 260 m	Misbit – Oman hyperalkaline spring	Detection limit (µM)
Na^+ (mM)	12.136	12.302	6.747	2.12	0.013
Ca^{2+} (mM)	6.424	7.604	9.001	0.017	0.008
Mg^{2+} (mM)	0.005	0.06	0.655	6.54	0.014
K^+ (mM)	0.409	0.422	0.361	–	0.039
$SiO_{2(aq)}$ (mM)	0.011	0.007	0.016	0.04	0.498
Cl^- (mM)	24.942	25.932	21.848	6.97	0.564
SO_4^{2-} (mM)	0.483	0.19	0.05	0.07	0.208
NO_3^- (mM)	0.012	0.022	0.016	<0.01	0.806
Br^- (mM)	0.001	<0.001	0.001	–	0.626
Al^{3+} (mM)	0.098	0.086	0.045	0.023	0.259
Fe^{2+} (mM)	<0.001	<0.001	<0.001	<0.001	0.004
DIC (mM)	0.091	0.078	0.391	–	–
H_2 (mM)	0.18	0.67	0.17	–	0.01
CH_4 (mM)	1.44	0.17	0.04	–	0.01
Ni (µM)	0.147	0.137	0.156	–	0.000
As (µM)	0.042	0.04	0.047	–	0.004
Se (µM)	0.094	0.144	0.166	–	0.002
Cu (µM)	0.032	0.04	0.045	–	0.001
Cd (µM)	<8.90E−05	<8.90E−05	<8.90E−05	–	0.000
Zn (µM)	0.028	0.056	0.139	–	0.001
Co (µM)	0.006	0.005	0.007	–	0.000
Cr (µM)	0.163	0.17	0.19	–	0.005

The fluids in both wells are hyperalkaline: NSHQ14 has a pH of 11.5 and NSHQ04 has a pH of 10.6. Major cation and anion analysis for fluids reveals >6 mM Ca^{2+}, ⩾0.005 mM Mg^{2+}, and 6.75–12.30 mM Na^+ (Table 1). Low molecular weight organic acids (lactate, acetate, formate, propionate, butyrate and valerate) are below detection limits of ∼5.0 µM; thus, there is low dissolved organic carbon in the fluid. Dissolved inorganic carbon (DIC) levels for samples collected from these wells in 2012 were 0.078–0.391 mM (Paukert et al., 2012). Both wells contain high concentrations of Cl^- (>20 mM), which are almost two orders of magnitude higher than the 0.35 mM Cl^- present in Oman rainwater (Weyhenmeyer, 2000, Paukert et al., 2012). The well fluids contain 0.05–0.48 mM SO_4^{2-} and 0.012–0.022 mM NO_3^-. The trace

element chemistry of the wells is similar; Ni and Cr are the most abundant metals (average of 0.15 and 0.18 μM, respectively. The only notable difference is NSHQ14 at 262 m has more Zn (0.139 μM versus ~0.03 μM) than the other depths.
The fluids in the peridotite wells exhibit similar pH and aqueous geochemistry to surface alkaline springs previously sampled in Oman (Paukert et al., 2012); however, the NSHQ14 and NSHQ04 well fluids contain more Ca^{2+}, Cl^{-}, NO_3^{-} and generally SO_4^{2-}. The dissolved silica concentrations are ~0.01 mM $SiO_{2(aq)}$ versus the 0.04 mM found in the surface seeps.
Oxidation-reduction potential (ORP) values were measured during the January 2012 field season. NSHQ14 fluids exhibit much higher ORP values (−31.6 mV) near the surface at 18 m, whereas the fluids at 260 m are highly reducing (−597.3 mV). The ORP value for fluids collected from NSHQ04 at 70 m was −103.4 mV.

3.2. Isotopic composition of fluids, dissolved gases, and carbonates

The δD values of dissolved H_2 are very low (−680‰ and −686‰ for NSHQ04 and NSHQ14 respectively, Table 2). The $\delta^{18}O$ of the well waters are −3.0‰ and 0.7‰ and the δD values are −15‰ for NSHQ04 and 2‰ for NSHQ14. If the dissolved H_2 formed in isotopic equilibrium with the water, we calculate a temperature of formation of ~50 °C using the theoretical geothermometer developed by Bottinga (1969). The δD values of CH_4 are also low, −205‰ and −232‰ for NSHQ04_18m and NSHQ14_262m, respectively. In contrast, the CH_4 is strongly enriched in ^{13}C ($\delta^{13}C$ CH_4 for NSHQ04_18m is +2.4‰; NSHQ14_262m is +3‰) (Table 2). These $\delta^{13}C$ CH_4 and δD CH_4 values from Oman subsurface fluids are notably higher than previously defined isotopic fields for thermogenic, biogenic, and abiotic methane (Fig. 2). The carbonate found in the drill cuttings $\delta^{13}C_{VPDB}$ ranges from −1.48 to −7.05‰ while the $\delta^{18}O_{VPDB}$ ranges from −7.73 to −11.49‰ (Table 3). The carbonate concentrations in the rock were low and not quantified.

Table 2. δD H_2, $\delta^{13}C$ CH_4, and δD CH_4 values for subsurface well water in Oman (NSHQ04 and NSHQ14), as well as hyperalkaline surface springs in Oman (Neal and Stanger, 1983), Zambales Ophiolite in the Philippines (Abrajano et al., 1990), Lost City Hydrothermal Vents (Proskurowski et al., 2006), the Precambrian Canadian Shield (Sherwood Lollar et al., 1993), and the Cedars Ophiolite in California (Morrill et al., 2013).

	δD H_2 ‰	δD CH_4 ‰	$\delta^{13}C$ CH_4 ‰
NSHQ04_18m	−680	−205	2.4
NSHQ14_262m	−685	−232	3
Nizwa, Oman	−697		

	$\delta D\ H_2$ ‰	$\delta D\ CH_4$ ‰	$\delta^{13}C\ CH_4$ ‰
Bahla, Oman	−699		
Huwayl Qufays, Oman	−699		
B'lad, Oman	−714		
Zambales Ophiolite	−581	−122	−7.34
Lost City Hydrothermal Vents	−609	−127	−10
Precambrian Canadian Shield	−619	−284	−29
Cedars ophiolite	−40 to −50		−68

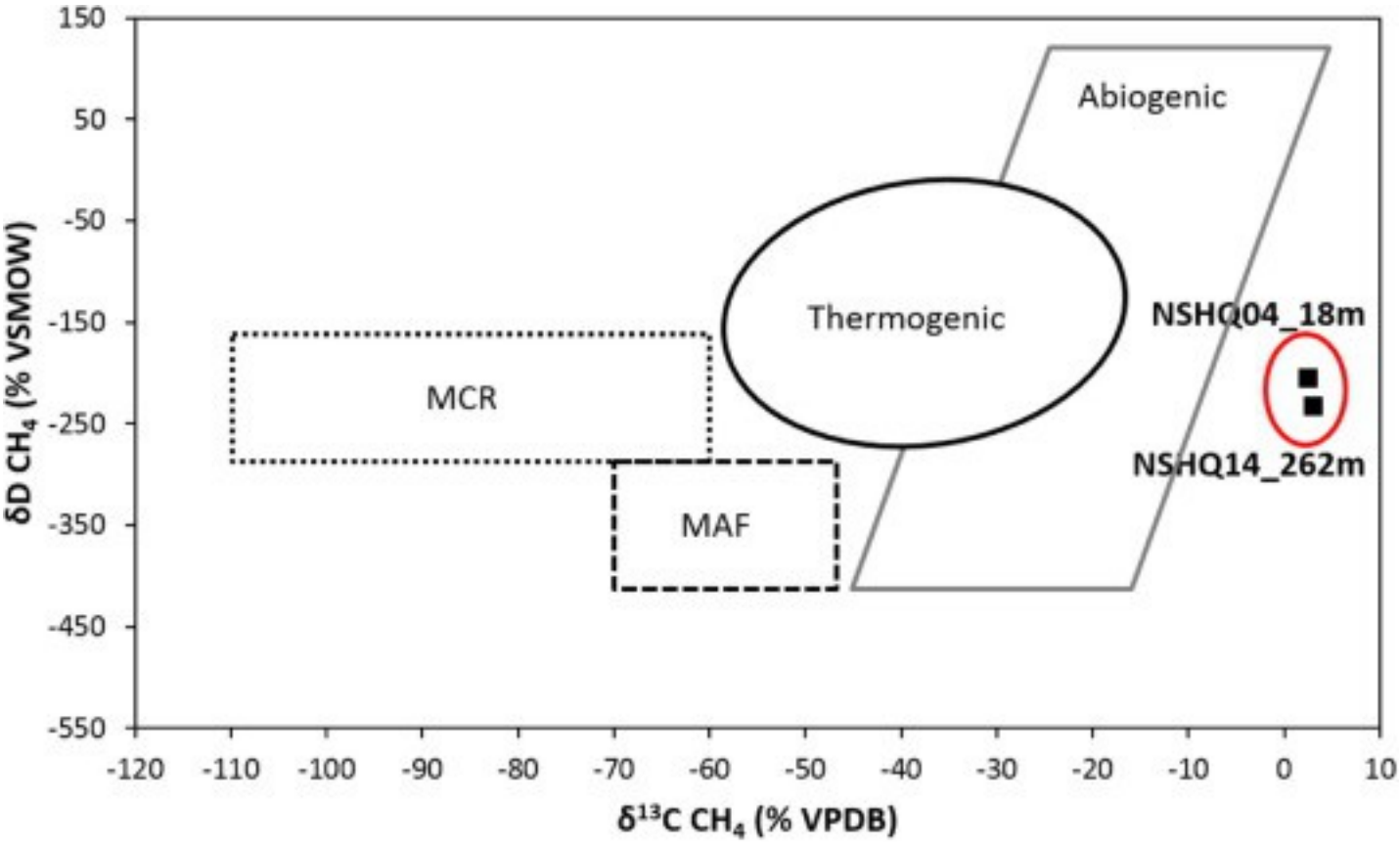

1. Download high-res image (121KB)
2. Download full-size image

Fig. 2. CH_4 isotope variation derived from deuterium and carbon isotopic data. MCR: microbial CO_2 reduction, MAF: microbial acetate fermentation (Etiope et al., 2013). Abiogenic red box drawn from variety of abiogenic sources (Abrajano et al., 1990, Sherwood Lollar et al., 1993, Etiope et al., 2011, Etiope et al., 2013, Laier and Nytoft, 2012) Thermogenic methane values encompass range of various thermogenically derived gases (Whiticar, 1990). Yellow circle surrounds values (black squares) obtained from subsurface hyperalkaline wells in Oman. (For interpretation of

the references to color in this figure legend, the reader is referred to the web version of this article.)

Table 3. $\delta^{13}C$ and $\delta^{18}O$ values from carbonate found in drill cuttings. The unreported values are due to low carbonate concentrations.

	$\delta^{13}C_{VPDB}$	$\delta^{18}O_{VPDB}$
NSHQ14_17m	−7.05	−7.73
NSHQ14_70m	–	–
NSHQ14_140m	−4.75	−11.07
NSHQ14_262m	−4.69	−11.49
NSHQ04_120m	–	–
NSHQ04_180m	–	–
NSHQ04_303m	−1.48	−10.99

3.3. Mineralogy of drill cuttings

Bulk powder XRD spectra are similar between the two wells. They are dominated by lizarditeand enstatite and contain magnetite near the surface (Fig. 3A and B). In the drill cuttings at 70, 140, and 262 m from NSHQ14, there is a brucite peak at 18.8 2θ, but not at the shallow 17 m. NSHQ04 drill cutting XRD spectra also contain a brucite peak at depth (180 and 303 m), but not at 120 m. There is a magnetite peak at 35.5 2θ in the NSHQ14 drill cuttings at 17 and 70 m and in the NSHQ04 drill cuttings at 120 and 180 m.

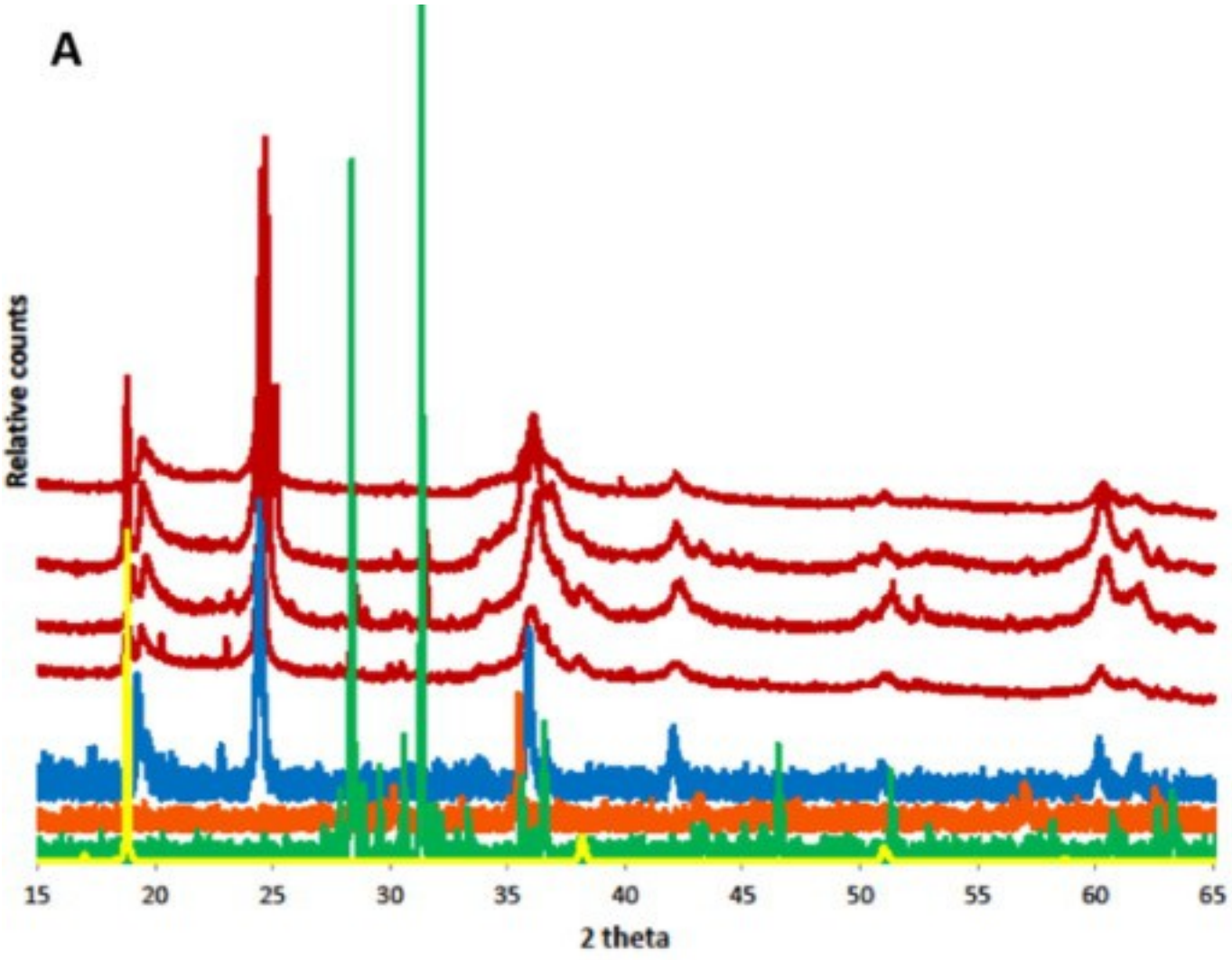
A
Relative counts
15
20
25
30
35
40
45
50
55
60
65
2 theta

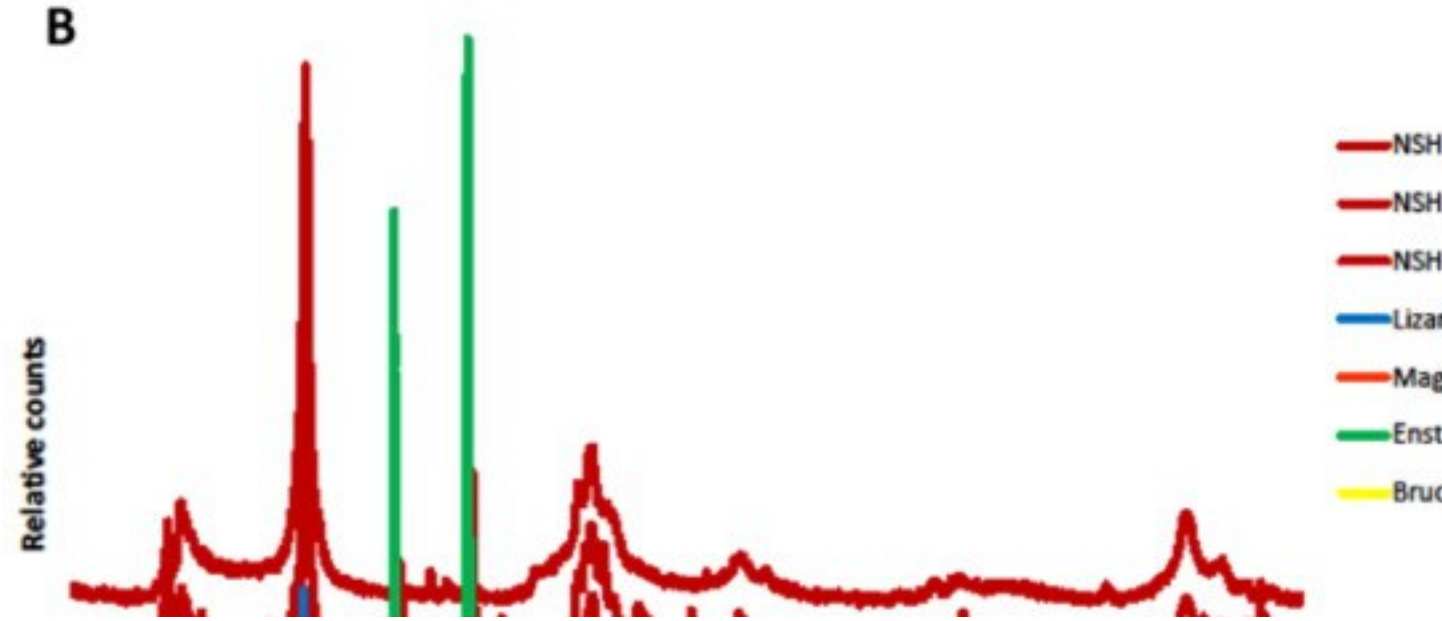
B
Relative counts
NSH
NSH
NSH
Liza
Mag
Enst
Bruc

1. Download high-res image (438KB)
2. Download full-size image

Fig. 3. (A) NSHQ14 powder XRD data from 4 well chip depths (in red, top 17 m down to 262 m). Lizarditepeaks (blue spectrum) match best to drill cuttings (RRUFFID = 60006). Enstatite peaks (green) also match well (RRUFFID = 040093). Sharp peak centered at 18.8 corresponds to brucite (yellow, RRUFFID = 050455). Magnetite (orange, RRUFFID = 060656) peak at 35.5 is evident in drill cuttings closer to the surface. (B) NSHQ04 powder XRD data from 3 well depths (in blue, 120 m well chip on top and go down with depth to 303 m). Lizardite peaks (blue spectra) match best to drill cuttings (RRUFFID = 60006). Enstatite peaks (green) also match well (RRUFFID = 040093). Sharp peak centered at 18.8 corresponds to brucite (yellow, RRUFFID = 050455). Magnetite (orange, RRUFFID = 060656) peak at 35.5 is evident in drill cuttings closer to the surface. Both powder XRD datasets show increasing magnetite towards surface. (For interpretation of the references to color in this figure legend, the reader is referred to the web version of this article.)

Microscale mineralogical structure and chemistry of drill cuttings were determined by a combination of petrologic observations, Raman microspectroscopy, Fe K-edge XANES spectroscopy and electron microprobe analyses. Olivine, diopside, enstatite, chromite, magnetite, brucite, and two-three different generations of serpentine, both chrysotile and lizardite, were detected in the drill cuttings of both wells using Raman microspectroscopy (Fig. 4). Brucite and olivine are not detected in the drill cuttings closer to the surface, approximately <120 m. The NSHQ14 drill cuttings become increasingly serpentinized as they approach the surface, showing decreasing relict olivine with proximity to the surface and increasing serpentine (Fig. 5). The NSHQ04 drill cuttings also show increased serpentine closer to the surface. There are visually more pyroxenes present in NSHQ04, both diopside and enstatite (Fig. 6), and they appear to be partially fractured and altered (lower left corner of Fig. 5). Drill cuttings from both wells have magnetite veins and grains (~5 μm) between 17 and 120 m deep.

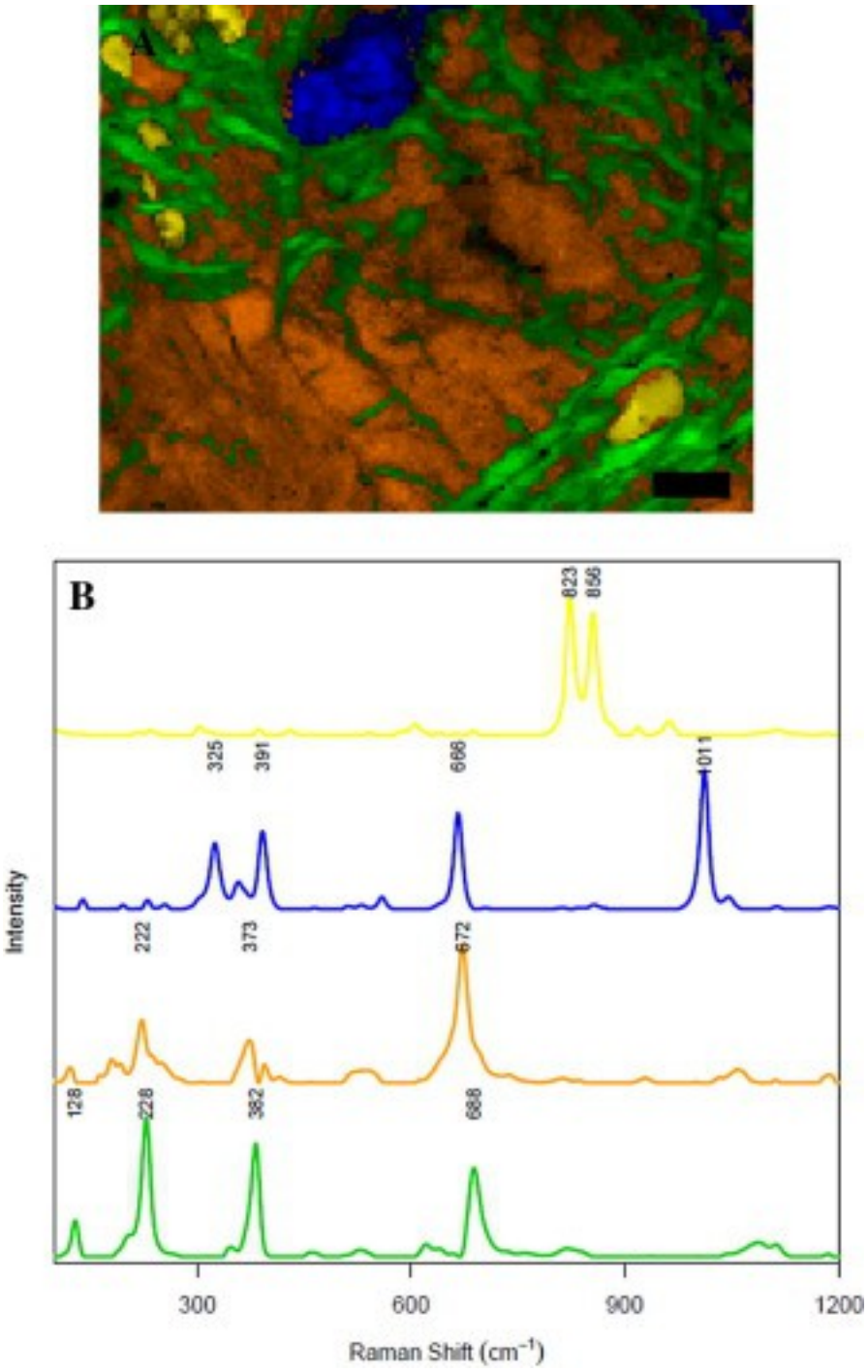

1. Download high-res image (212KB)
2. Download full-size image

Fig. 4. (a) Map of NSHQ14_262m thin section mineralogy generated using Raman spectroscopy and multivariate curve resolution-alternating least square (MCR-ALS). Lizardite (green, 14-gen2) is crosscutting an older generation of lizardite (orange, 14-gen1). Other components in the map include olivine (yellow) and diopside (blue).

Scale bar 50 μm (b) Raman spectra for each component shown in map (a). Variation in peak position is due to orientation effects. (For interpretation of the references to color in this figure legend, the reader is referred to the web version of this article.)

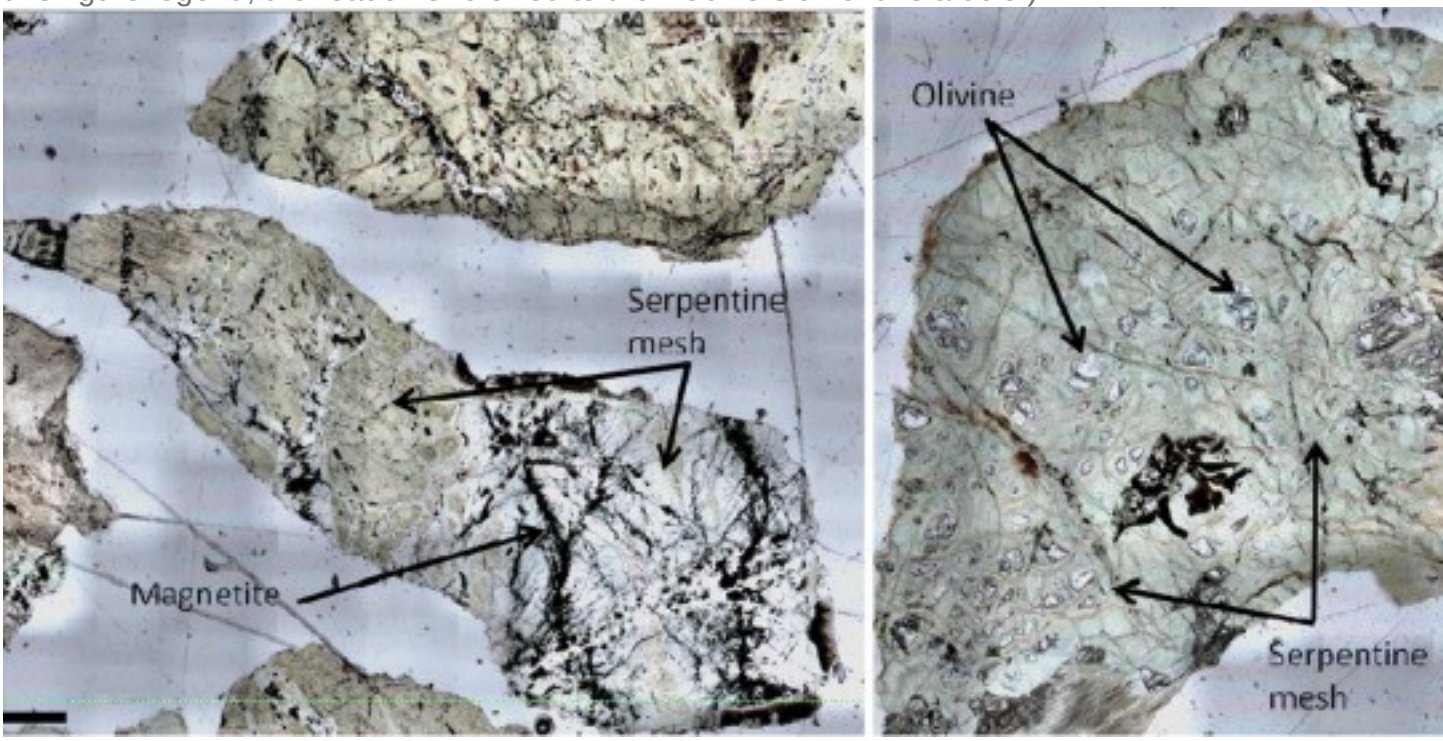

1. Download high-res image (486KB)
2. Download full-size image

Fig. 5. NSHQ14_17m (left) heavily serpentinized mesh texture with extensive magnetite veins compared to NSHQ14_262m with relict olivine (right). Scale bar 400 μm.

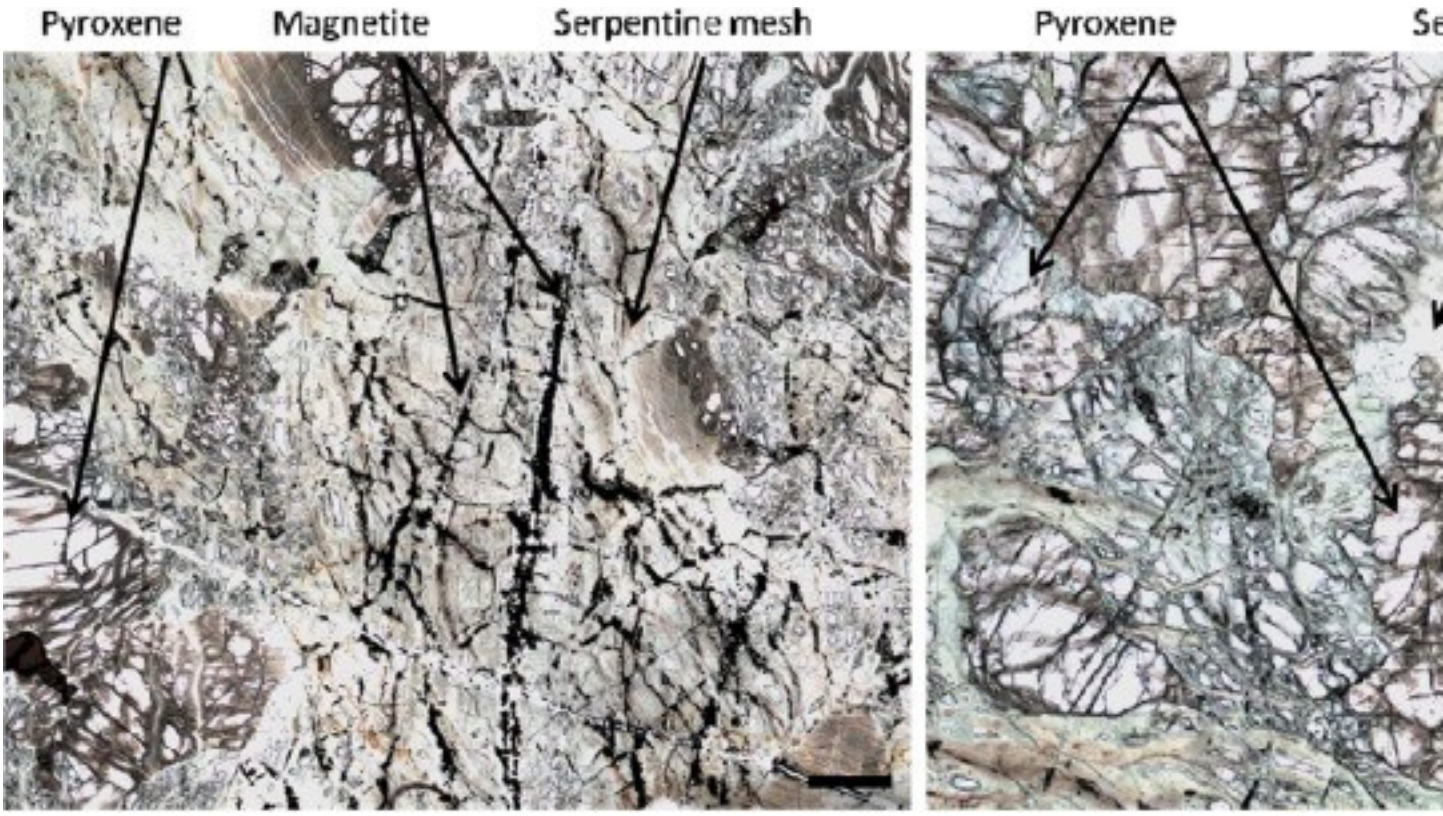

1. Download high-res image (655KB)
2. Download full-size image

Fig. 6. NSHQ04_120m well chip showing relict pyroxene with extensive magnetite veins compared to NSHQ04_180m showing large pyroxene grains and limited magnetite. Scale bar 400 μm.

The Raman maps demonstrate that the drill cutting mineralogy is dominated by two to three generations of serpentine. Although chrysotile, lizardite, and antigorite can be identified by Raman spectroscopy from their varying peak positions (Rinaudo et al., 2003, Groppo et al., 2006, Petriglieri et al., 2015), differences in peak position are relatively small and can be obscured by large crystal orientation effects on the relative peak intensities. Furthermore, the effects of varying Mg/(Mg + Fe) and Fe^{3+}/Fe_T on the Raman spectra for the serpentine polytypes are not yet well quantified. Thus, it is difficult to determine the polymorphs of serpentine with certainty when just looking at the fingerprint region from 90 to 1600 cm^{-1}. By mapping the serpentine in both the fingerprint region of 90–1600 cm^{-1} and in the more diagnostic O-H stretching region of 3400–3800 cm^{-1}, different regions of serpentine have been identified as chrysotile and lizardite (Fig. 7C).

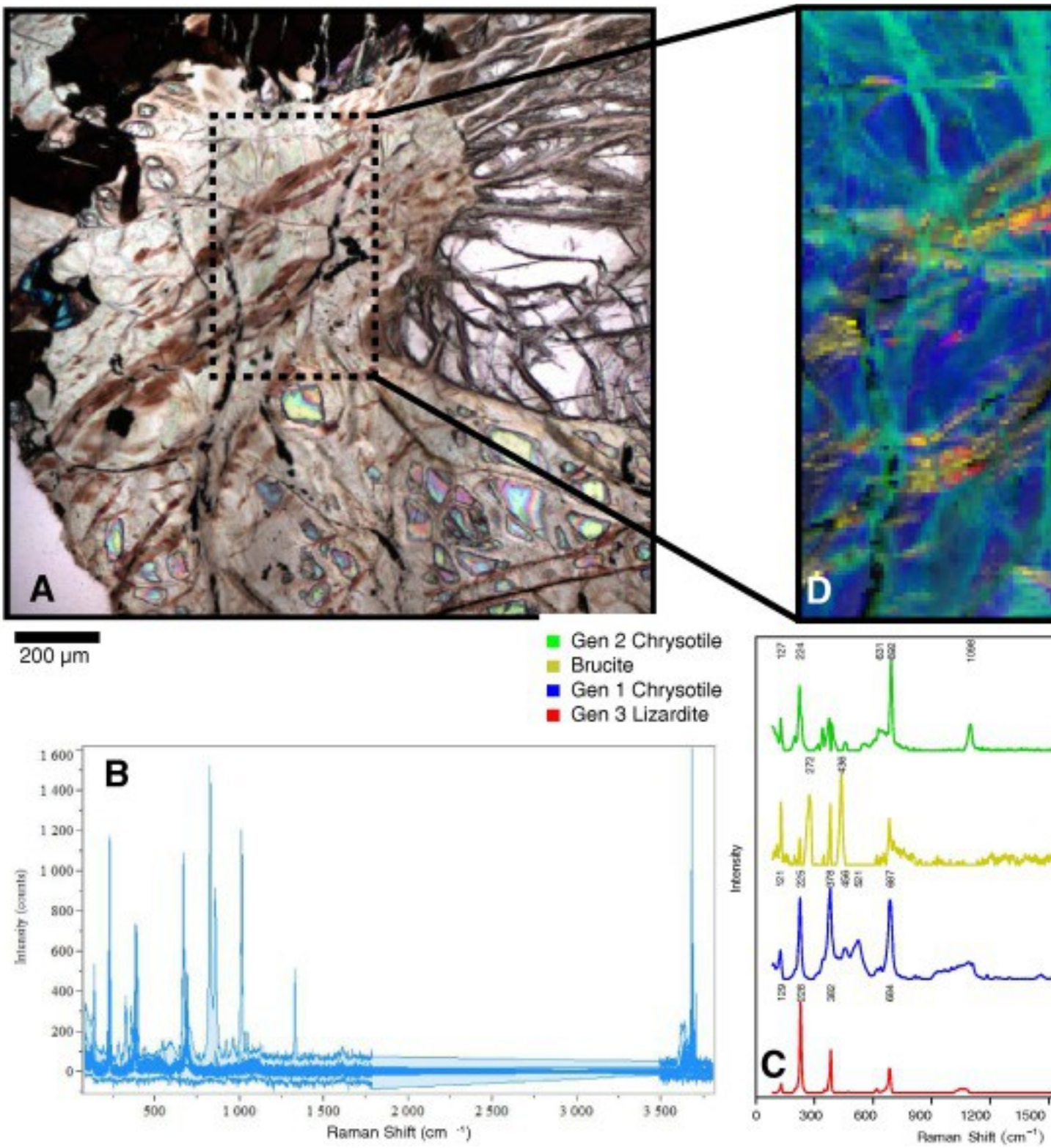

1. Download high-res image (957KB)
2. Download full-size image

Fig. 7. Micro-Raman mapping of well chip NSHQ04 at 180 m depth. (A) Thin section image in transmitted light shows black magnetite surrounded by brown serpentine crosscutting background lighter serpentine. (B) Shows all 14,529 spectra from map in “fingerprint” region between 90 and 1800 cm^{-1} and the O–H stretch from 3400 to 3800 cm^{-1}. (C) We identified 4 distinct spectra for the major alteration minerals using MCR. Blue is generation 1 chrysotile (04-gen1) overprinted by green generation 2 chrysotile (04-gen2). These are both overprinted by the intermixed red generation 3 lizardite (04-gen3) and yellow brucite (D) These spectra were then fit to the entire map region. (For interpretation of the references to color in this figure legend, the reader is referred to the web version of this article.)

Crosscutting relationships reveal distinct generations of serpentine. NSHQ14 at 262 m contains two generations of lizardite with an older lizardite (14-gen1) crosscut by a younger lizardite (14-gen2) (Fig. 4). NSHQ04 at 180 m has a complex alteration history with a first generation of chrysotile (04-gen1) overprinted by a younger second generation of chrysotile (04-gen2). Brucite is intermixed with third generation lizardite (04-gen3). The intermixed lizardite and brucite are visually apparent in plane polarized light as brown veins (Fig. 7). All depths contain multiple generations of serpentine with chrysotile overprinted by lizardite that is variably intermixed with brucite. The drill cuttings closer to the surface contain less chrysotile and more lizardite. There is more brucite at depth than closer to the surface, as evidenced by powder XRD and Raman spectroscopy. Brucite is visually associated with brown serpentine as seen in Fig. 7. Both NSHQ14 and NSHQ04 drill cuttings contain widespread magnetite (Fig. 8) as identified by Raman microscopy. The magnetite forms both veins and 2–10 μm specks, in some cases in elongate patches or veins cross-cutting all generations of serpentine. Some magnetite is associated in veins with lizardite, but we can use cross-cutting relationships to infer that some of the magnetite postdates formation of all other alteration minerals in these drill cuttings. There is more magnetite observed closer to the surface.

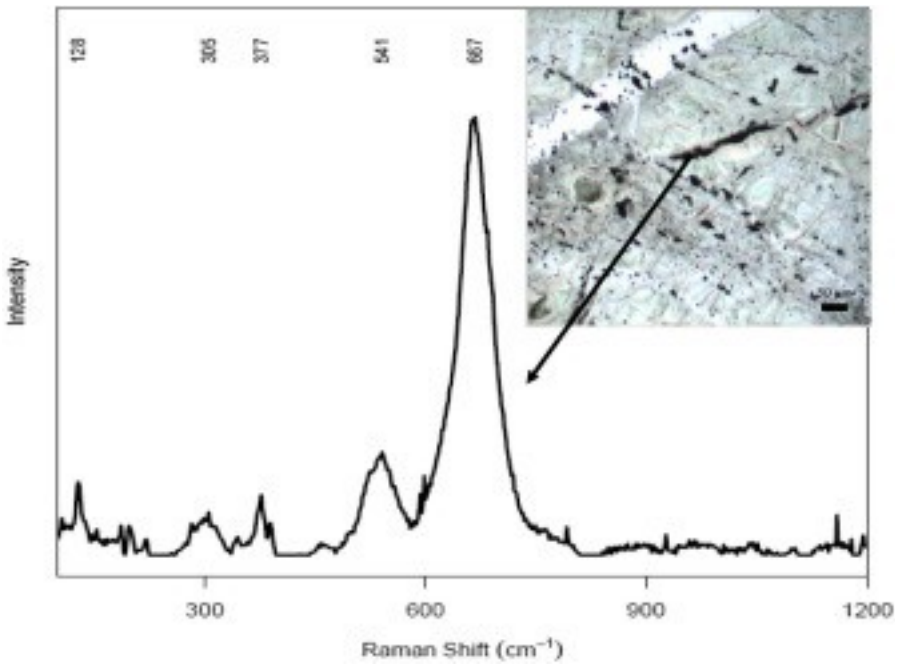

1. Download high-res image (135KB)
2. Download full-size image

Fig. 8. Raman spectra from NSHQ04_120m; magnetite veins (black veins and specks) as identified by Raman spectra. Magnetite is cross-cutting all generations of serpentine.

The chemical variation between generations of serpentine in well chip NSHQ04_180m was quantified with electron microprobe (Table 4). Generations 04gen1 and 04-gen2 chrysotile are chemically identical and contain high amounts of trace metals, notably an average of 0.67 wt% Al_2O_3, 0.22 wt% MnO and 0.33 wt% Cr_2O_3 whereas generation 04-gen3 lizardite has less than 0.07 wt% of those elements. Generation 04-gen3 lizardite has more MgO (40.90 wt% versus 36.06 wt%) and less SiO_2 (34.60 wt% versus 36.87 wt%) than the chrysotile. The totals are low for the serpentine, possibly due to the presence of brucite intermixed with serpentine as well as due to structural water.

Table 4. Electron microprobe weight % data for serpentine generations from well chip NSHQ04_180m corresponding to varying generations of serpentine identified with Raman spectroscopy. Numbers refer to various analysis spots on the well chip thin section.

Generation 1 and 2 chrysotile (04-gen1,2)						
Sample	**3**	**5**	**6**	**9**	**10**	**Average**
Na_2O	0.00	0.00	0.00	0.00	0.04	0.01
MgO	36.41	35.22	36.17	36.86	35.63	36.06
Al_2O_3	0.40	0.99	0.82	0.31	0.85	0.67
SiO_2	38.21	35.97	36.40	36.70	37.05	36.87

Generation 1 and 2 chrysotile (04-gen1,2)						
Sample	**3**	**5**	**6**	**9**	**10**	**Average**
CaO	0.40	0.54	0.44	0.30	0.47	0.43
FeO	7.29	8.50	7.51	8.12	8.20	7.92
MnO	0.20	0.26	0.18	0.14	0.32	0.22
TiO_2	0.00	0.00	0.00	0.00	0.00	0.00
Cr_2O_3	0.09	0.61	0.51	0.00	0.42	0.33
Total	82.99	82.09	82.03	82.43	82.99	82.51
Mg #	0.83	0.81	0.83	0.82	0.81	0.82
Generation 3 lizardite intermixed with brucite (04-gen3)						
Sample	7	8	11	12	13	Average
Na_2O	0.00	0.00	0.00	0.00	0.00	0.00
MgO	41.00	41.01	40.93	40.74	40.84	40.90
Al_2O_3	0.00	0.00	0.08	0.14	0.03	0.05
SiO_2	33.58	34.51	35.74	34.63	34.54	34.60
CaO	0.06	0.07	0.12	0.15	0.12	0.10
FeO	8.12	7.41	6.07	6.13	7.24	6.99
MnO	0.00	0.00	0.11	0.09	0.15	0.07
TiO_2	0.00	0.00	0.00	0.00	0.00	0.00
Cr_2O_3	0.00	0.00	0.00	0.00	0.00	0.00
Total	82.76	83.00	83.05	81.88	82.93	82.72
Mg #	0.83	0.85	0.87	0.87	0.85	0.85

We tried to quantify the amount of brucite and serpentine in the drill cuttings with TGA analysis (e.g. Lafay et al., 2012). We first measured known amounts of serpentine and brucite separately, and then mixed the two minerals to verify the method (Supplementary Fig. 1). The resulting spectra and mass estimates are found in Supplemental information. From this test, we see that mixtures of serpentine and brucite are not reliable for determining the mass of both minerals. Thus, we did not utilize TGA as a technique for quantifying the mass of serpentine and brucite.

3.4. Fe speciation within the drill cuttings

When comparing bulk Fe-XANES of the drill cuttings to the bulk spectra of a partially serpentinized dunite (OM95-35) from Oman, the drill cutting spectra are more oxidized as noted by the shift in the spectral features to higher energies (Fig. 9). Also, the drill

cutting spectra are more oxidized than San Carlos olivine, the type specimen characteristic of unaltered olivine. However, it is difficult to discern differences in the Fe-XANES spectra and Fe-speciation (i.e. average oxidation states and mineralogy) between well depths (Fig. 9).

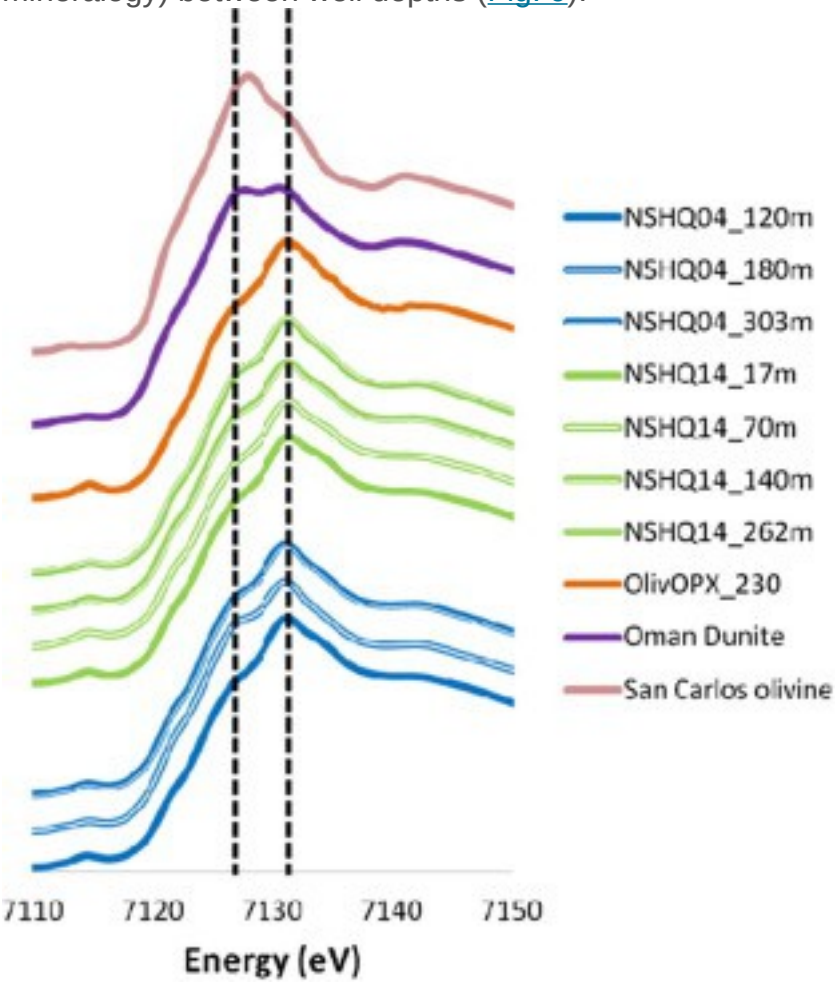

1. Download high-res image (141KB)
2. Download full-size image

Fig. 9. Bulk Fe K-edge XANES data for all depths of NSHQ14 and NSHQ04. Representative spectra of partially serpentinized dunite from Oman, XANES spectra of San Carlos olivine (type specimen of unaltered olivine), and OlivOPX_230 (serpentine formed during laboratory alteration of olivine and pyroxene with water at 230 °C) are also shown.

The bulk Fe-XANES spectra of the drill cutting samples were fit by Fe XANES model spectra (e.g. Mayhew et al., 2011) of known minerals in the sample: olivine, pyroxene, brucite, magnetite, and serpentine. The linear-combination fits to the data show that serpentine increases in the higher drill cuttings, and olivine and brucite decreases, while

pyroxene remains relatively constant (Supplementary Table 3). The changes in bulk Fe speciation are small and due to the number of Fe-bearing phases present, the bulk Fe XANES data is relatively insensitive to noted mineralogical changes such as increased magnetite. We did not collect a highly resolved pre-edge for the bulk XANES data; thus, it was not possible to quantify a shift in Fe(II)/Fe(III) with depth.

We obtained Fe K-edge μXANES spectra from the multiple generations of serpentine (as identified from Raman spectroscopy) to determine variations in Fe-oxidation state and coordination within serpentines across samples. Three distinct Fe K-edge serpentine spectra with varying oxidation states are shown in Fig. 10. Focusing on the pre-edge (7108–7118 eV) reveals the unoccupied states of the Fe 2p orbital, giving insight into both oxidation state and coordination (Wilke et al., 2001, Andreani et al., 2013). The serpentine spectra have a shift in the centroid position in the pre-edge to higher energy, which reveals that there is a significant Fe(III) component. In addition, the increase in the fluorescence intensity at higher energy indicates that some of this Fe(III) is tetrahedrally coordinated. The spectra with the prominent second peak at 7130 eV most closely aligns with the lizardite generation identified by Raman, whereas the most shifted spectrum (prominent peak ~7130.5 eV) is associated with the chrysotile. The spectrum most shifted to lower energy is San Carlos olivine − a reduced spectrum that contains only Fe^{2+} (Fig. 10). The ferric to ferrous iron ratio could not be quantitatively calculated using the method of Wilke et al., 2001, Andreani et al., 2013, and Muñoz et al. (2013) because these data were collected on a Beamline 2-3 at SSRL using a Si 110 vs. 311 monochromator, resulting in poorer energy resolution. This shifts and broadens the pre-edge features relative to published standards. However, such quantification will be possible in the future by measuring the same standards across multiple beamlines through inter-laboratory exchange.

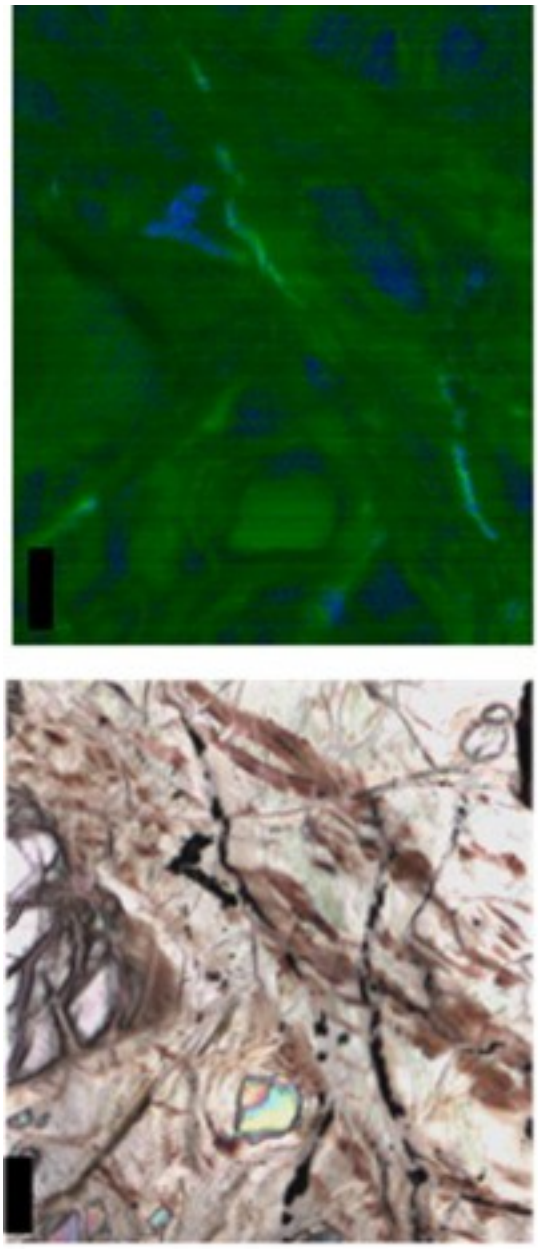

1. Download high-res image (276KB)
2. Download full-size image

Fig. 10. NSHQ04_180m Multiple energy Fe-K edge fitted map of serpentine variation. Two distinct serpentine Fe K-edge XANES spectra (green, blue) from 7108 to 7148 eV, red spectra shows San Carlos olivine. The inset shows a zoomed-in pre-edge (7108–7118 eV) environment, revealing that the blue and green spectra contain oxidized Fe(III) with tetrahedral component as seen by the prominent peak around 7114.5 eV. Black scale bar is 90 μm. (For interpretation of the references to color in this figure legend, the reader is referred to the web version of this article.)

3.5. Magnetic hysteresis analysis of the drill cuttings

The drill cuttings exhibit two distinctive types of hysteresis behavior. Drill cuttings deeper than 120 m are paramagnetic while those shallower than 120 m are ferromagnetic (Table 5). The ferromagnetic samples (NSHQ14_17m, NSHQ14_70m, and NSHQ04_120m) also show superparamagnetic behavior, indicating that a population of the magnetic minerals in the samples are smaller than magnetically stable single-domain size particles, likely <20 nm (Dunlop, 1973, Butler and Banerjee, 1975, Worm, 1998). We also note a large increase in the saturation magnetization values in the drill cuttings closer to the surface than at depth in both NSHQ04 and NSHQ14 samples (Table 5).

Table 5. Room temperature magnetic hysteresis measurements. Grain size is detected from the hysteresis curve of each sample; hysteresis parameters obtained from modeled curve by QuickMagIC (Tauxe et al., 2014).

Well depth	Magnetic types	Hysteresis behavior	Saturation magnetization(A * m^2)	Remanent magnetization (A * m^2)	Saturation coercivity (T)	Coercivity (T)
NSHQ14_17m	Ferromagnetic	Super-paramagnetic	0.000151	0.000021	0.034300	0.011600
NSHQ14_70m	Ferromagnetic	Super-paramagnetic	0.000277	0.000023	0.034300	0.007960
NSHQ14_140m	Paramagnetic		0.000028	0.000004	0.033900	0.012900
NSHQ14_262m	Paramagnetic		0.000033	0.000004	0.036000	0.013550
NSHQ04_120m	Ferromagnetic	Super-paramagnetic	0.000359	0.000031	0.032900	0.008517
NSHQ04_180m	Paramagnetic		0.000057	0.000011	0.030500	0.014260
NSHQ04_303m	Paramagnetic		0.000191	0.000025	0.033600	0.011200

3.6. 16S rRNA analysis of DNA collected from well fluids

We sequenced the hypervariable V4–V5 region of the 16S rRNA gene from DNA extracted from filters that were loaded with biomass by pumping fluids from each well. Analysis of the 16S rRNA data shows that the NSHQ14 16S sequences were 99.5% bacteria and 0.05% archaea. Similar dominance of bacterial sequences was observed in NSHQ04 (99.4% bacteria and 0.06% archaea). The Bacteria are dominated by members of the Deinococcus-Thermus, Nitrospirae, Firmicutes, Chloroflexi, and Proteobacteria phyla. Fluids from both wells contain candidate phylum OP1 (1.1% and 2.8%, respectively), and NSHQ04 additionally has candidate phylum OD1. The species

richness, as determined by the number of OTUs from each well, is 1737 for NSHQ04 fluids vs. 710 for NSHQ14. NSHQ04 is more diverse than NSHQ14.
We found that *Meiothermus* (phylum Deinococcus-Thermus, class Deinococci) comprises 8.6% (NSHQ04) and 46.1% (NSQH14) of the operational taxonomic units (OTUs) in both wells. *Thermodesulfovibrionaceaea* (phylum Nitrospirae), a sulfate-reducer, comprises 21.6% of NSHQ14 and 1.4% of NSHQ04. Chloroflexi is prominent in NSHQ04, 5.3%, but only 0.1% in NSHQ14 (Table 6). Both wells contain Firmicutes (class Clostridia family Anaerobrancaceae), fermentative microorganisms, and Proteobacteria (genus Hydrogenophaga), hydrogen-oxidizing bacteria found in other serpentinizing systems (Brazelton et al., 2013, Suzuki et al., 2013). The fluids from both wells notably contain methanogen *Methanobacterium*, which can utilize hydrogen and variable carbon sources such as formate to produce methane. *Methylococcus*, a methanotroph, is also present. Full taxonomy, OTU, and sequence data can be found at: https://dx.doi.org/10.6084/m9.figshare.1544535.v1.

Table 6. Heat map of relative abundance of top OTUs from 16S rRNA sequencing of filtered well waterfrom NSHQ04 and NSHQ14. Red indicates the highest number of OTUs, green indicates the lowest number of OTUs. Phyla, class, and order of best-fit OTUs are shown. The “other bacteria” correspond to OTUs that could not be matched to any known bacteria. The “remaining bacteria and archaea” corresponds to all OTUs that comprise <1.0% of the total OTUs.

NSHQ04	NSHQ14	Phyla	Class	Order
8.6%	46.1%	Deinococcus-Thermus	Deinococci	Thermales
1.4%	21.6%	Nitrospirae	Nitrospira	Nitrospirales
7.2%	0.0%	Firmicutes	Clostridia	Natranaerobiale
5.8%	0.4%	Proteobacteria	Gammaproteobacteria	Methylococcale
6.0%	0.0%	Proteobacteria	Betaproteobacteria	Burkholderiales
4.7%	0.0%	Bacteroidetes	Bacteroidia	Bacteroidales
3.5%	0.1%	Chloroflexi	TK17	mle1-48
2.4%	1.2%	Proteobacteria	Alphaproteobacteria	Rhodospirillale
2.3%	0.6%	Proteobacteria	Deltaproteobacteria	Desulfovibriona
0.6%	2.2%	GAL15		
2.8%	0.0%	OP1	OPB14	
2.3%	0.1%	Proteobacteria	Gammaproteobacteria	Chromatiales
2.4%	0.0%	Proteobacteria	Betaproteobacteria	Rhodocyclales
0.6%	1.8%	Proteobacteria	Betaproteobacteria	Burkholderiales
2.2%	0.0%	Firmicutes	Clostridia	Desulforudales
0.2%	1.7%	Firmicutes	Clostridia	Natranaerobiale
1.9%	0.0%	Proteobacteria		
1.8%	0.0%	Chloroflexi	Anaerolineae	Anaerolineales
0.7%	0.9%	Proteobacteria	Betaproteobacteria	Burkholderiales
1.2%	0.0%	Other bacteria (unclassified)		
0.0%	1.1%	OP1	MSBL6	
1.0%	0.0%	Thermus-Deinococcus	Deinococci	Deinococcales
1.0%	0.0%	Firmicutes	Clostridia	
1.0%	0.0%	Other bacteria (unclassified)		
38.4%	22.4%	Remaining bacteria and archaea<1.0%		

4. Discussion

This study explores the mineralogy and aqueous geochemistry of modern water/rock reactions associated with low temperature serpentinization and hydrogen production in Oman and how these processes may give rise to habitable conditions for microbial life in the peridotite aquifer. We then use 16S rRNA sequencing of DNA extracted from subsurface fluids to investigate the phylogenetic diversity of the fluid microbial communities and infer potential microbial metabolisms sustained in-situ.

4.1. Fluid chemistry of low temperature serpentinization

Modern alteration of primary minerals in the aquifer is evident from the abundant Ca^{2+} and OH^- in peridotite hosted well waters NSHQ04 and NSHQ14 (Neal and Stanger, 1983, Neal and Stanger, 1984, Neal and Stanger, 1985). Neal and Stanger, 1983, Neal and Stanger, 1984, Neal and Stanger, 1985 extensively studied the hydrogeology of Oman's fluids and coined these hyperalkaline waters (pH > 11) containing Ca^{2+}–$2OH^-$ as Type II fluids, following the initial observation of Barnes and O'Neil (1969). They are situated in serpentinized dunite and harzburgite and are derived from serpentinization reactions with subsurface fluids that are isolated from the atmosphere. The hydration of olivine and pyroxene causes the water to become enriched in Ca^{2+}–OH^- (Barnes and O'Neil, 1969, Neal and Stanger, 1984, Bruni et al., 2002, Kelemen et al., 2011):

(2)$4Mg2SiO4+CaMgSi2O6+7H2O=3Mg3Si2O5OH4+Ca2++2OH-$

The Ca^{2+} is released from diopside (present in all drill cuttings), and then accumulates in the water because Ca^{2+} is not incorporated into serpentine minerals (Barnes et al., 1967). These Type II fluids are carbon-depleted and when they emerge at surface springs, they rapidly mix with atmospheric carbon dioxide to precipitate carbonate minerals (Stanger, 1986, Kelemen and Matter, 2008, Kelemen et al., 2011, Paukert et al., 2012, Mervine et al., 2014). The Ca^{2+}values we measure in the deeper subsurface fluids are ~1 mM higher than those reported from hyperalkaline springs, presumably because Ca^{2+} in the subsurface has not been depleted through the precipitation of carbonate minerals. Thus, sampling the Type II fluids in wells before they interact with atmospheric CO_2 in the unsaturated zone or on the surface provides a more direct assessment of the water composition in the aquifer.

The subsurface well water contains more Cl^- than found in Oman rainwater and hyperalkaline surface seeps (Paukert et al., 2012) which provides additional proof that modern water/rock interaction is occurring. We infer that the high Cl^- concentrations are due to the presence of Cl^- that was incorporated in the Oman peridotite during initial, high-temperature serpentinization near an oceanic spreading ridge, and dissolved in groundwater during ongoing weathering (Stanger, 1986). The Cl^- is presumably at lower concentrations at the surface seeps than in the wells because it is precipitating with carbonates in salt.

The wells only contain Type II fluids; however, the shallow peridotite aquifer in Oman also hosts Mg^{2+}–$2HCO_3^-$ as observed by Barnes and O'Neil (1969). These are termed Type I fluids (Neal and Stanger, 1983, Kelemen et al., 2011) and are moderately alkaline fluids of a Mg^{2+}–$2HCO_3^-$ composition found in the shallow groundwater (~pH 8–9). In Oman, Type I fluids are typically found in wadi (channel that is dry except during rainy seasons) pools, ultramafic wadi gravels, and water wells (e.g., Neal and Stanger,

1985, Paukert et al., 2012) and form through the following simplified reaction (e.g. Kelemen et al., 2011):

(3)$Mg_2SiO_4+4CO_2+2H_2O=2Mg^{2+}+4HCO_3^-+SiO_2$

Atmospheric carbon dioxide dissolves in the water and forms bicarbonate as olivine and serpentine minerals in the near-surface react with the waters and release magnesium ions and silica. Although we did not observe Type I fluids in this study, their mixing and interaction with Type II fluids may be influencing water/rock reactions and microbial diversity in the subsurface. In particular, the presence of oxygenated Type I fluids in the highly fractured upper portion of the aquifer may explain the aerobic organisms detected by 16S rRNA sequencing.

4.2. Mineral assemblages associated with low temperature hydrogen production

We investigated the mineralogy of the subsurface aquifer to see if the mineral assemblages give insight into the water/rock reactions and mechanisms that produce hydrogen at low-temperature. The drill cuttings contain serpentine, brucite, and magnetite, as is common in partially serpentinized peridotites. Although the drill cuttings are heavily serpentinized, they still contain relict olivine at depth that diminishes towards the surface, which suggests olivine may be the dominant mineral reacting with the in-situ fluids. There is a significant portion of unaltered pyroxene that could also be reacting; however, few zones of pyroxene alteration have been observed. Pyroxene alteration can be a dominant reaction in other serpentinizing sites (Klein et al., 2009, Marcaillou et al., 2011, Andreani et al., 2013). A common alteration product of pyroxene is talc [$Mg_3Si_4O_{10}(OH)_2$] under conditions of high silica activity (Frost and Beard, 2007, McCollom and Bach, 2009, Klein et al., 2013a). We do not observe any talc formation; thus, we do not believe pyroxene alteration is dominating the water/rock reactions, although the high concentrations of Ca^{2+} in the fluids do suggest that at least some pyroxene dissolution is occurring in the hyperalkaline aquifer.

The multiple generations of serpentine observed in the drill cuttings reveal that the mantleperidotite experienced multiple periods of water/rock alteration. The mantle section of the ophiolite was first serpentinized near an oceanic spreading ridge, during emplacement of the ophiolite onto the Arabian continental margin, and/or during subaerial erosion and a subsequent marine transgression in the late Cretaceous (Kelemen and Matter, 2008, Hanghøj et al., 2010, Mervine et al., 2014). These events may have caused formation of the extensive chrysotile matrix seen in the drill cuttings. The chrysotile is overprinted by lizarditeveins; however, we cannot infer a

formation temperature due to the fact that chrysotile is metastable relative to lizardite (Evans, 2004).

We characterized the Fe content and speciation of the serpentine to investigate reservoirs of Fe in the system. Both the lizardite and chrysotile contain ~7–8 wt% FeO_T (considering all Fe as Fe^{2+}). In average natural samples, chrysotile contains 3 wt% FeO_T, while lizardite ranges from 2 to 8 mol.% Fe (Evans et al., 2009, Streit et al., 2012). Thus, the chrysotile in Oman is Fe-rich while the lizardite is average. Characterization of serpentine in our samples with electron microprobe and XANES confirms the presence both Fe(II) and Fe(III) in the serpentine. Fe(III) can substitute into both the octahedral and tetrahedral sites, replacing Si^{4+}, to form cronstedtite, $(Mg_2,Fe^{3+})_3(Fe^{3+},Si)_2\ O_5(OH)_4$ (Frost and Beard, 2007, Klein et al., 2009, Evans, 2010, Streit et al., 2012). The formula for chrysotile inferred during early alteration of the peridotite is $(Mg_{2.79}Fe^{II}_{0.10}Fe^{III}_{0.11})(Si_{1.89}Fe^{III}_{0.11})O_5(OH)_4$ while the younger lizardite formula is difficult to determine because it is intermixed with brucite. It contains less Si (perhaps due to intergrown brucite) than the chrysotile, but has high Fe concentrations (6–8 wt% FeO_T), with Fe occupying both tetrahedral and octahedral sites.

Fe(III) rich serpentine forms at low temperatures (<200 °C) (Streit et al., 2012, Klein et al., 2013a) and may have played an important role in hydrogen generation in Oman because it is another reservoir of oxidized Fe (besides magnetite), that can form during Fe(II)-driven reduction of water to form hydrogen. Generally, the oxidized Fe(III) is assumed to partition into magnetite (Eq. (1)). However, at lower temperatures, there is a decreasing thermodynamic drive for magnetite formation (Klein et al., 2013a), and indeed magnetite may redissolve into serpentine at low temperature (Streit et al., 2012). Thus, Fe(III)-rich serpentine becomes an important mineral to consider as an indicator of hydrogen production during serpentinization (Klein et al., 2009, Marcaillou et al., 2011, Andreani et al., 2013). The average oxidation state of Fe in the drill cuttings is greater than that of partially serpentinized dunite from Oman and San Carlos olivine (Fig. 9). This reveals rocks interacting with hyperalkaline fluids have been altered after their initial formation when they contained mostly Fe(II). Moreover, spatially-resolved Fe K-edge XANES data on drill cuttings reveal the presence of Fe(III)-rich serpentine. Our observation of Fe(III) rich serpentine is consistent with observations from Streit et al. (2012) of Fe(III)-rich serpentine in Oman rocks undergoing low-temperature alteration processes, and from Andreani et al. (2013) during serpentinization at mid-ocean ridges (<150–200 °C).

We find that in addition to Fe(III)-rich serpentine, magnetite is also formed during low-temperature serpentinization in Oman in the upper portions of the two wells studied. The

simplified unbalanced Eq. (6) presented in Klein et al. (2013b) shows how magnetite and Fe(III)-rich serpentine can accommodate hydrogen production:

(4)(MgFe)2SiO4+vH2O=w(MgFeII)OH2+x(MgFeII/III)3(SiFeIII)2O5(OH)4+yFe3O4+zH2

Such reactions may contribute to the high levels of H_2 found in the subsurface fluids. As noted above, and demonstrated in Fig. 8, there is extensive magnetite in our samples, with some of it forming veins that cross-cut all of the serpentine assemblages. Downhole bulk sample magnetic hysteresis analyses indicate that the drill cuttings above 70 and 120 m in NSHQ14 and NSHQ04 wells (respectively) are ferromagnetic (i.e. minerals that retain remnant magnetization) and have superparamagnetic grain sizes, further confirming that there is increased magnetite in drill cuttings closer to the surface. The drill cuttings at depth, on the other hand, have a paramagnetic signature (i.e. no retainable magnetic properties without applied field). The hysteresis behavior (Tauxe et al., 2014) shows there are multiple size populations of magnetite in these rocks (micron-scale and nanoscale magnetite), or the visible magnetite particles must consist of aggregations of nano-scale magnetite.

The measured changes in magnetic character augment the petrological observation of increased magnetite population closer to the surface. It is possible to calculate an approximate mass of magnetite in the sample using an empirically derived constant of 92 A m^2/kg to correlate the saturation magnetization with the amount of magnetite (Malvoisin et al., 2012). However, such a quantification of magnetite assumes that the magnetic carrier in the sample is equal to and/or larger than single-domain size magnetite particles. This assumption may be false in our samples. Hysteresis analysis of each sample clearly exhibits significant contribution from superparamagnetic particles, which means the field will never be fully saturated, which effectively underestimates the amount of magnetite present in the drill cuttings. In addition, there is a prevalence of FeII/III-bearing serpentine grains also mixed within the matrix. Instead, we simply utilize the suite of magnetic data to show several lines of evidence indicating increased magnetite formation at shallow depths.

Brucite can accommodate Fe(II) in its structure that can then be oxidized during subsequent alteration to produce hydrogen at low temperatures (Klein et al., 2013a). Typically, brucite forms mesh rims around olivine and traps Fe(II) in a stable mineral structure and prevents hydrogen generation (Klein et al., 2009, Evans, 2010). However, in our drill cutting samples, and in our comparison Oman dunite sample, we observe brucite intimately intermixed with lizardite. It is not possible to determine an iron content for the brucite due to the fact that it is not present in large enough, serpentine-free areas for analysis. Electron microprobe measurements were not used to constrain Fe-

contents of brucite intermixed with serpentine because Fe can substitute into Si sites in serpentine (particularly in Fe(III) rich serpentine) as well as Mg sites in brucite, thus an estimate of brucite calculated from electron microprobe would be inaccurate. However, Raman analysis shows a distinct change in the brucite spectrum from that of the pure $Mg(OH)_2$ endmember. Additionally, brucite in serpentinizing systems commonly contains iron; brucite can include greater than 10 wt% FeO_T, with increasing Fe content at lower temperatures in the same bulk composition (Moody, 1976, Klein et al., 2009). Yet brucite is not thermodynamically stable at the silica activities measured in our fluid samples (Table 1). Thus, we propose that brucite should react with silica-rich fluids in the aquifer (Bach et al., 2006), driving Fe(II) to undergo oxidation to form Fe(III)-rich serpentine and/or magnetite while concurrently reducing H_2O to make H_2 (see Eq. (7) below).

There are several possible reasons for the high silica activity in our fluid samples. First, the fluids in the wells are high in Ca^{2+}. Well NSHQ04 is close to the Moho, the zone of contactbetween peridotite and gabbro. Thus, it is possible gabbro-equilibrated fluids are interacting with the peridotite aquifer. Fluid that has equilibrated with gabbro has higher silica activity, and it will destabilize and consume brucite (Frost and Beard, 2007). However, there is insufficient hydrological information about the region surrounding the wells to test this hypothesis, and the similarity of fluids in wells NSHQ04 (near the Moho) and NSHQ14 (kilometers from the Moho) seems inconsistent with this hypothesis.

Bach et al. (2006) suggest that high Si fluids are generated when olivine nears exhaustion in the host rock and pyroxene alteration becomes a more important control on fluid chemistry. This is plausible given the low amount of relict olivine remaining in the drill cuttings.

A third possibility, as shown in Eq. (3), is that the generation of Type I waters in the shorter residence fluid-flow pathways can lead to fluids with high silica activities. Subsequently, we may be observing the destabilization of brucite in the host rock when Type I waters mix with Type II fluids within the shallow subsurface. This is supported by the observation of decreasing brucite in the highly serpentinized samples near the surface where Type I waters may be present.

There is increased extent of serpentinization in the drill cuttings near the surface as opposed to at depth, which suggests varying hydrological pathways in the subsurface. The top tens of meters below the surface could be subject to more variable conditions with higher water/rock ratios and/or interaction with Type I fluids than rock at depth due to rainwater recharge. This can lead to increased fracture permeability (e.g., Kelemen and Hirth, 2012) and periodic exposure to oxygen, as well as shorter fluid residence

times. Thus, the fluids will not be equilibrated with the mineral assemblages, leading to more rapid destabilization and alteration, as well as increased oxidation and drive to form magnetite.

4.3. Hydrogen generating reactions

Based on our observations, we infer that three different hydrogen generating reactions have occurred in the subsurface. An initial serpentinization stage prior to modern water/rock reactions produced hydrogen from alteration of olivine and led to the production of Fe(II)-bearing brucite and Fe(III) rich serpentine (chrysotile generation):

(5)$MgFeII2SiO4+H2O=xMgFeIIOH2+yMgFeII/III3SiFeIII2O5(OH)4+zH2$

There is relict olivine in the deep drill cuttings that is replaced by serpentine at shallower depths, so similar H_2 generating reactions could occur today. Moreover, less brucite might form because modern silica activities in the fluids are too high for brucite stability. Thus we suggest that relict olivine is now reacting to form new Fe(III)-bearing lizardite and hydrogen at low temperatures:

(6)$(MgFeII)2SiO4+H2O=xMgFeII/III3SiFeIII2O5(OH)4+yH2$

Currently, a high silica fluid is interacting with the rock, destabilizing the Fe(II)-bearing brucite (as modeled in Geochemist Workbench). This leads to the formation of magnetite and lizardite, with the production of hydrogen:

(7)$(MgFeII)(OH)2+SiO2=xFeIIFe2IIIO4+yMgFeII/III3SiFeIII2O5(OH)4+zH2$

The destabilization of Fe(II)-bearing brucite to form magnetite and serpentine, and the alteration of olivine to Fe(III) rich serpentine, should both produce hydrogen at low temperatures. This model of alteration and hydrogen generation is consistent with observations by Andreani et al. (2013) that serpentinites from mid-ocean ridges contain both Fe(III)-serpentine and more magnetite as the degree of serpentinization increases.

4.4. Isotopic signature of hydrogen and methane

The isotopic signature of the H_2 serves as a valuable indicator of formation temperature, which complements mineralogical observations of serpentinization leading to hydrogen production. (Neal and Stanger, 1983) collected gas samples from surface hyperalkaline seeps and observed low δD H_2 values (−697‰ and −714‰) similar to those measured from our well samples (−680‰ and −686‰). They noted that H_2- and CH_4-rich gases (H_2 as high as 99% and CH_4 as high as 4.3%) emerge at hyperalkaline surface seeps, whereas the well fluids provide access to dissolved gases in the host rock itself. Abrajano et al., 1990, Sherwood Lollar et al., 1993, and Proskurowski et al.

(2006) also found negative δD gases that formed at low temperatures (<200 °C) at other serpentinizing sites (both continental and oceanic), as shown in Table 4.

The dissolved gases from Oman subsurface wells uniformly contain some of the most negative δD hydrogen gas found in nature. We calculate a formation temperature of ∼50 °C by applying the geothermometer of Bottinga (1969) to the coupled δD H_2 and δD H_2O in the well fluids. Assuming the geothermal gradient at NSHQ14 is approximately 25 °C/km (Paukert et al., 2012), the gases are hypothesized to form at a depth of less than 2 km. A formation temperature of ∼50 °C supports the hypothesis that low-temperature serpentinization and hydrogen formation is occurring in the Oman aquifer, rather than H_2being physically released from hydrogen inclusions that formed during higher temperature serpentinization events (McCollom and Seewald, 2001). We verified the lack of gas-rich inclusions in relict olivine by extensively probing the olivine grains by confocal Raman spectroscopy. However, the mantle section of the ophiolite is up to 8 km thick (Ravaut et al., 1997); thus, the H_2 could be generated at temperatures as high as 200 °C and then migrate upwards to the surface. In this case, the current negative δD of the H_2 could instead represent isotopic exchange and re-equilibration between the H_2 and H_2O after formation of the H_2 as the waters circulate to shallower, cooler depths.

NSHQ04 fluids contain millimolar amounts of CH_4, which may be produced abiotically due to the highly reducing conditions reflected in the abundant H_2 in the system. In olivine dissolution reactions at 30+ °C, (Neubeck et al., 2011) observed measureable CH_4, potentially through the oxidation of H_2 and reduction of CO_2 (Sleep et al., 2004). However, the CH_4 detected by Neubeck et al. (2011) could have been released from fluid inclusions, or produced by reaction of fluid with the experimental reaction vessel. At higher temperature (>120 °C), CH_4 production can occur abiotically through Fischer–Tropsch-type or Sabatier reactions, through catalysis by magnetite and awaruite (Ni–Fe alloy) commonly found in serpentinites (Frost, 1985, Lorand, 1987, Horita and Berndt, 1999). Etiope et al. (2013)suggested catalysts such as ruthenium or chromite produce methane at temperatures <50 °C. Such low temperature methane production may be possible in Oman due to the abundance of magnetite, chromite and awaruite found in the partially serpentinized mantle peridotites. Alternatively, methane formation could be biologically mediated by methanogens.

The $\delta^{13}C$ CH_4 signatures are the highest values reported in the literature thus far despite the wide range of methane isotopic compositions compiled in the past 30+ years. Plots comparing the ranges of $\delta^{13}C$ CH_4 and δD CH_4 found in various geologic environments (Whiticar, 1990, Etiope et al., 2013) give context to methane isotopic compositions

measured in the peridotite-hosted wells in Oman. Thermogenic natural gas has been extensively studied, as have gases from extreme environments like hyperalkaline lakes and Antarctic ice sheets (Whiticar, 1990). The previously highest documented $\delta^{13}C$ CH_4 values (−1.6‰) were found from the Ilimaussaq inclusions Greenland (Laier and Nytoft, 2012, Etiope et al., 2013). That methane was hypothesized to have a biological origin, and subsequent sediment burial and partial loss by diffusion during uplift and erosion enriched the gas in isotopically heavy methane (Laier and Nytoft, 2012). A similar explanation is plausible for the high $\delta^{13}C$ CH_4 values in Oman. Alternatively, if the methane we observe in Oman formed abiotically at 50 °C at a depth of ∼2 km, similar to the H_2, slow diffusion upwards from depth could fractionate and enrich the remaining methane in isotopically heavy carbon after the lighter ^{12}C CH_4 has diffused away. However, this should have a similar effect on the hydrogen isotopic composition of the methane as well, which we did not observe. The methane-hydrogen D/H fractionation can be used to estimate temperature of formation of methane (Horibe and Craig, 1995) at ∼70° ± 3 °C.

The isotopic composition of methane collected from wells in Oman falls near the traditionally defined abiotic range. Abiotic methane tends to have $\delta^{13}C$ CH_4 values greater than −50‰ and δD of CH_4 can range from −450 to −50‰ (Etiope and Sherwood, 2013, Etiope et al., 2013). Bacterial reduction of CO_2 to methane gives negative $\delta^{13}C$ CH_4 values as low as −110‰ and δD CH_4 down to −531‰ (Whiticar, 1999); thus, methane from Oman does not have a traditional bacterial signature. Low temperature CH_4 production has been experimentally demonstrated with ruthenium and rhodium catalysts (Jacquemin et al., 2010). Platinum group metal inclusions, including Ru and Rh, are found in chromites (e.g., Jacquemin et al., 2010). Platinum group metals in chromites in Oman could be catalyzing low temperature methane formation and leading to a heavy $\delta^{13}C$ CH_4 signature, but there are no experimental data to confirm this hypothesis. High ^{13}C CH_4 can also be produced by extensive biological oxidation of biogenic or abiogenic methane that enriches the residual methane in ^{13}C (Whiticar and Faber, 1986, Whiticar, 1999); however, this would also be expected to enrich δD in the residual methane. Thus, if methane cycling is active in the subsurface aquifer, the isotopic signature of CH_4 may not be an unequivocal marker of the methane formation pathway (Whiticar and Faber, 1986, Templeton et al., 2006).

The processes giving rise to the heavy $\delta^{13}C$ CH_4 in Oman cannot be elucidated without further investigation of the microbial and low-temperature abiotic pathways that are giving rise to the production of mM concentrations of CH_4. First, the source of carbon must be assessed. The $\delta^{13}C$ signature of carbonates mineralized in Oman peridotites

provide some insights into the isotopic signature of the carbon pool. The carbonate found in the drill cuttings $\delta^{13}C$ ranges from −1.48 to −7.05‰ while the $\delta^{18}O$ is −7.73 to −11.49‰. These values are similar to the Mg-rich carbonate veins from outcrops and roadcuts that have $\delta^{13}C$ ranging from −25.98 to 0.98‰ and $\delta^{18}O$ from −7.04 to 5.56‰ (Clark and Fontes, 1990, Kelemen and Matter, 2008, Kelemen et al., 2011, Mervine et al., 2014). The negative $\delta^{13}C$ values as low as −26‰ probably formed through a mechanism dominated by kinetic isotope fractionation during carbonate precipitation. Both the values from the drill cuttings and outcrops are still lighter than $\delta^{13}C$ in the CH_4, suggesting that even if the entire DIC pool was converted to methane under extreme carbon limitation, processes such as further $\delta^{13}C$ enrichment by diffusion or partial oxidation of the methane must be invoked.

4.5. Potential metabolic pathways supported by hyperalkaline fluids

The hyperalkaline fluids in Oman contain electron donors and acceptors to sustain anaerobic microbial metabolisms. There are millimolar amounts of H_2 and CH_4 to serve as electron donors, but dissolved organic acids were not detected at the micromolar detection limit. NSHQ04 notably contains high levels of SO_4^{2-}, which may be a source of critical electron acceptors for microorganisms (ex. sulfate reducers). Nitrate found in both wells is another potential electron acceptor that can be coupled with oxidation of H_2, CH_4 and Fe(II).

The aqueous geochemistry of the well fluids can support several potential metabolic pathways. Well fluids contain more sulfate and nitrate than samples from hyperalkaline seeps with comparable pH, and elevated H_2 and CH_4 (Paukert et al., 2012). Thus, nitrate and sulfate reduction at depth, tied to hydrogen oxidation, is likely. The high methane concentrations in NSHQ04 can support anaerobic oxidation of methane (AOM) (Hoehler et al., 1994, Joye et al., 2004), especially considering AOM consortia are often syntropically associated with sulfate-reducing microorganisms. The following reactions are often invoked for serpentinizing systems and may be relevant metabolisms for microbial life in the subsurface of Oman:

a.CO2(aq)+4H2(aq)=CH4(aq)+2H2O(l)

b.2NO3-+10Fe2++24H2O(l)=10Fe(OH)3+N2+18H+

c.NO3-+2.5H2(aq)+H+=0.5N2(aq)+3H2O(l)

d.SO42-+4H2(aq)+2H+=H2S(aq)+4H2O(l)

e.CH4(aq)+SO42-=HCO3-+HS-+H2O(l)

f.CH4(aq)+4NO3-=CO2(aq)+4NO2-+2H2O(l)

(Hoehler et al., 1994, Nielsen and Nielsen, 1998, Chapelle et al., 2002, Cardace and Hoehler, 2009, Haroon et al., 2013, Cardace et al., 2015). These metabolic strategies provide the energy to generate an electrochemical gradient to produce ATP. However, it is energetically taxing to generate a traditional hydrogen pump at high pH (Hicks et al., 2010, Suzuki et al., 2014). Microorganisms in Oman may be employing a sodium or calcium motive force to generate ATP instead of a proton pump. Many microorganisms pump H^+ ions outside the cell to create an energy gradient, but in a high pH environment, this H^+ quickly combines with abundant OH^- in the environment and cannot be utilized by the cell. Microorganisms can adapt to hyperalkaline conditions by generating a sodium motive force instead of pumping protons onto the surface of a cell inundated with OH^-. There is ample Na^+ in the fluids, so organisms in Oman may use a sodium motive force to cope with high pH environments. Alternatively, recent work has shown that some organisms can utilize a proton motive force, even under alkaline conditions (Mulkidjanian et al., 2008, Hicks et al., 2010, Suzuki et al., 2014). The pH in NSHQ04 is slightly lower than in NSHQ14, potentially making it more habitable for microorganisms. NSHQ04 also has more abundant electron donors, nitrate and sulfate, than NSHQ14, further increasing its habitability.

4.6. Organisms detected in fluids from 16S rRNA sequencing

Predictions about potential metabolic pathways in serpentinizing systems aid in interpreting 16S rRNA data from the fluids and allow us to place the phylogeny of the organisms detected in the subsurface fluids within a context of potential functional activities. There is a curious mixture of both aerobic and strictly anaerobic microorganisms in the subsurface. DNA extracted from well fluids shows the presence of aerobic organisms *Meiothermus* and *Hydrogenophaga* that require oxygen as an electron acceptor. *Meiothermus* is considered to be obligately aerobic and chemoorganotrophic, capable of utilizing a range of carbon sources from glucose to acetate (Tindall et al., 2010). *Hydrogenophaga* is chemoorganotrophic or chemolithoautotrophic, and it oxidizes hydrogen and reduces organic material or heterotrophically denitrifies nitrate (Willems et al., 1989). We also found members of the Clostridia class and *Methanobacterium* genera, which are strict anaerobic fermenters and methanogens, respectively. Anaerobes *Thermodesulfovibrionaceaea* are also present, which are sulfate reducing bacteria that use hydrogen as electron donors and ferment pyruvate or other organics (Haouari et al., 2008). We likely significantly mixed the deep and shallow well fluids during pumping, so there may be internal variation in

the fluid Eh as a function of depth, and intervals of variable permeability, that affect microbial community composition and function in ways that we cannot yet identify. The near-surface fluids probably have a shorter residence time and more recent interaction with ambient atmospheric oxygen. The mixture of organisms may point to an upper zone of more oxidized fluids in the wells (e.g. Type I fluids), leading to an interesting geochemical interfaces that microorganisms can exploit.

Methanobacterium, a methanogen, is present in NSHQ04 and NSHQ14. This may explain the abundant CH_4 in the wells. It is a strict anaerobe that oxidizes H_2 and reduces formate, CO, or CO_2 to produce methane (Balch et al., 1979).

Similar *Methanobacterium* sequences have also been observed in the Zambales ophiolite seeps (Woycheese et al., 2015). Methanogenesis is oftentimes invoked as a metabolic pathway in serpentinizing environments due to the abundant hydrogen and methane in the fluids (Chapelle et al., 2002, Cardace and Hoehler, 2009, Cardace et al., 2015). In order to determine *Methanobacterium*'s contribution to the CH_4 in the wells, it will be necessary to investigate the abundance and activity of the methanogens along with the isotopic signature of the CH_4that they produce.

Candidate phylum OP1 was first detected in hot springs, but curiously it is present in the mesophilic, hyperalkaline conditions of the Oman subsurface. OP1 was first found in a neutral hot spring (75–95 °C) in Yellowstone rich in iron, sulfide, carbon dioxide, and hydrogen (Kumar and Saravanan, 2011). There is a nearly complete genome for the OP1 *Candidatus* 'Acetothermus autotrophicum' that suggests it is one of the earliest bacteria to branch from the last universal common ancestor (Takami et al., 2012). 13 of the OP1 OTUs from NSHQ14 have 100% identity to this genome, whereas the other 250 OP1 OTUs are other species from candidate phylum OP1. The genome for *Candidatus* 'Acetothermus autotrophicum' has a high GC content (61.9%), and this organism is estimated to have an ideal growth temperature of 84.7 °C. It also is phylogenetically similar to the members of the Deinococcus-Thermus clade, which is interesting giving the high concentrations of *Meiothermus* (phylum Deinococcus-Thermus) in the wells. The proposed metabolism of 'A. autotrophicum' is acetogenesis through the acteyl CoA pathway utilizing CO_2 and H_2, which is an ancient C-fixation pathway (Takami et al., 2012). Candidate phyla by definition are phyla with no cultured and formally described representative strains, so little to nothing is known about their metabolic requirements and physiology. Future microbiological studies of Oman subsurface fluids may provide more insight into the function of these organisms, particularly if they can be cultured and studied in the laboratory.

A diverse range of phyla were identified from the well fluids. Clostridia and *Hydrogenophaga*are abundant in the fluids, supporting the idea that previous studies probing hyperalkaline seeps were identifying organisms that are indeed present in the subsurface (Brazelton et al., 2013, Suzuki et al., 2013).

The *Hydrogenophaga* sequences detected here were 100% identical to *Serpentinomonas* (Suzuki et al., 2014), a bacterium cultured and characterized from the Cedars ophiolite. This organism is an obligate alkaliphile with an optimum growth pH of 11. It utilizes H_2, $CaCO_3$, and O_2 for growth. Clostridia, specifically members of the *Erysipelothrix* group, found in these samples were also found in the Tablelands Ophiolite, and this group is known to contain abundant fermentation-associated hydrogenases, suggesting that it uses organic compounds to survive (Brazelton et al., 2013). Lipidsextracted from brucite–calcite veins at the Iberia margin, a Lost-City type hydrothermal field, are also hypothesized to correspond to *Desulfotomaculum* and *Clostridium* (Klein et al., 2015); thus, Clostridia are widespread in serpentinizing systems. Additionally, these anaerobic organisms contain [FeFe]-hydrogenases that can catalyze hydrogen production from the reduction of organic materials like acetate and formate (Brazelton et al., 2012). Clostridia are also endospore-forming, which may allow them to persist in these fluids during nutrient-poor periods (Madigan, 2012).

The metabolic pathways of the 16S rRNA correspond to predictions of potential metabolisms in the fluids that are derived from the in-situ geochemistry. Chloroflexi have a range of metabolic strategies which include fermentation, CO_2 fixation, and acetogenesis (Hug et al., 2013). *Thermodesulfovibrionaceaea* is a sulfate-reducer, and some species of Clostridia may also be capable of sulfate reduction (Madigan, 2012). There are several Gammaproteobacteria in the fluids that may be denitrifiers (e.g. the extensively studied *Psuedomonoas stutzeri*) (Madigan, 2012). The other predicted metabolisms, such as methane oxidation and sulfate reduction, may be facilitated by Methylococcales and Desulfovibrionales.

The two wells host different microbial communities. This is most likely dictated by the varying geochemistry and pH between the subsurface systems. NSHQ04 has a lower pH (10.5) and more electron acceptors such as nitrate and sulfate to make it more habitable and diverse. NSHQ04 also has higher concentrations of CH_4 than NSHQ14, which is reflected by the fact that it contains methane oxidizers. Although our method of 16S rRNA amplicon sequencing does not reflect the quantity of organisms in the system, it does reveal that geochemistry strongly modulates microbial ecology in hyperalkaline subsurface fluids.

4.7. Carbon sources in hyperalkaline fluids

The well fluids from 2012 are carbon-poor with DIC concentrations that vary from 0.078 to 0.391 mM. It is possible that the highly reducing conditions produced by high levels of H_2 in serpentinizing environments lead to the abiogenic formation of low weight molecular acids (Lang et al., 2010, Schrenk et al., 2013). McCollom and Seewald (2001) observed formation of formate during 300 °C olivine serpentinization experiments:

(8)CO2+H2=HCOOH

High concentrations of formate (36–158 μm/kg) are observed at the Lost City Hydrothermal Field, and isotopic data suggest that the formate formed abiotically (Proskurowski et al., 2006, Lang et al., 2010). However, low molecular weight organic acids were not detected above the micromolar detection limit for the species measured in our samples, suggesting that they are not extensively produced under in-situ conditions. Alternatively, the absence of formate and other organic acids could be due to their rapid consumption by subsurface microorganisms.

We searched for complex organic carbon in the Oman drill cuttings as a potential carbon source and indicator of microbial life, but no accumulations of macromolecular carbon were detected in the well chips by Raman spectroscopy. Raman spectroscopic mapping has successfully been used to search for signs of life within serpentinized peridotites from the Mid-Atlantic Ridge, where complex organic carbon has been found in association with cavities in hydroandraditic garnets (Ménez et al., 2012). These hollow cavities are thought to host cryptoendolithic microbes, metabolizing H_2 generated through serpentinization or using Fe(III) in garnets as an oxidant for H_2. Complex organic molecules from these organisms might then migrate into the surrounding serpentines and ocean, providing a source of carbon for other microbial life (Pasini et al., 2013).

We also measured total organic carbon (TOC) in the drill cuttings through combustiontechniques, but the results are likely overestimates because residual magnesite may be present (Supplementary Table 1). Organic carbon could derive from a rock-hosted biome, but these concentrations of organic carbon could also be a relic of drilling contamination or abiotic reduction of CO_2. Further information about molecular structure and distribution of organic carbon are necessary to characterize its source.

Heavily altered Oman peridotites contain extensive carbonate vein networks (Kelemen and Matter, 2008, Kelemen et al., 2011, Streit et al., 2012, Paukert et al., 2012, Mervine

et al., 2014) which may provide an unconventional carbon source to microorganisms in the subsurface. Previous work by Suzuki et al. (2014) shows the *Serpentinomonas* can utilize $CaCO_3$ as a carbon source. However, we do not detect the presence of carbonate veins in the drill cuttings, but they are most likely a small component (aqueous carbonic acid was not measured) so would not be easily detected by bulk powder XRD. We did a simple test for carbonate by adding HCl and measuring change in mass and observe about 1% carbonate in the drill cuttings; this is also a low estimate, since the analysis is neglecting to measure magnesite. Thus, carbonate veins in the rocks may be a carbon source for organisms in the subsurface.

Finally, Type I, Mg–HCO_3-rich waters are abundant in Oman, and contain 1–10 mM total carbon (e.g., compiled data in Supplement of Kelemen and Matter, 2008). Type I waters could supply carbon for growth of micro-organisms by infiltration into more heavily reacted rocks hosting Type II waters.

5. Conclusions

Subsurface mantle peridotites from the Samail ophiolite in Oman are highly serpentinized and oxidized, and are in contact with hyperalkaline (>pH 10) fluids high in Ca^{2+}, OH^-, dissolved H_2 and CH_4. High concentrations of very negative δD H_2 values are inferred to have formed or equilibrated at ~50 °C. The coupled δD and positive $\delta^{13}C$ of the dissolved CH_4 would traditionally be interpreted as abiotic, and dissolved CH_4 has the most isotopically heavy $\delta^{13}C$ CH_4 reported in the literature thus far. We suggest that the methaneisotopic signature is in part modulated by significant oxidation, whether it was produced through biotic or abiotic pathways.

We hypothesize that these gas-rich hyperalkaline fluids have evolved through an ongoing stage of low temperature serpentinization in the peridotite. Olivine hydration during early hydrothermal alteration and obduction formed Fe(II,III) serpentine, Fe(II) brucite and hydrogen. During the current phase of low temperature water/rock interaction, brucite is destabilized in the fluids with high SiO_2 activity, generating H_2 when it is converted to magnetite and additional Fe(III)-rich serpentine. The relict olivine is also further reacting to form Fe(III)-rich serpentine and hydrogen. The formation mechanism for methane remains enigmatic, and could involve low temperature abiotic CO_2 reduction by mineral catalysts, or in-situ biological activity.

Our study of drill cuttings and fluids reveals that the timing and extent of various stages of serpentinization in Oman remain unconstrained. It is difficult to tease apart mineral parageneses formed during hydrothermal alteration near an oceanic spreading ridge, emplacement of the ophiolite, Late Cretaceous weathering, and modern

water/rock reactions. Future studies that can connect rock alteration histories along reaction paths with varying fluid sources and residence times will be a valuable next step in assessing the mechanisms and extent of modern, low-temperature H_2 and CH_4 generation. Continuous physical and magnetic properties measurements downhole and on bulk core samples will help delineate sections with hydrology *in situ* where serpentinization has been extensive.

16s rRNA data of DNA extracted from the hyperalkaline fluid microbial communities indicate an abundance of both aerobic and anaerobic organisms, including abundant *Meiothermus*, *Thermodesulfovibrionaceae* (sulfate-reducers), Clostridia (ferm entors), and *Hydrogenophaga* (H_2-oxidizers). Although not abundant, the methanogen*Methanobacterium* and candidate phylum OP1 are notably present. We hypothesize that the subsurface microbial communities are harnessing the H_2 produced by water/rock reactions, and coupling the oxidation of H_2 to electron acceptors such as SO_4^{2-}, CO_2 and Fe(III)-bearing phases at depth, and episodically with O_2 and nitrate in the upper fractured part of the aquifer.

Probing the microbial community composition in these fluids provides a first glimpse into the complex subsurface peridotite-hosted microbiome. The rock-hosted communities may be quite different than those established in the fluids, due to strong gradients in redox potential, electron acceptor and donor availability, porosity, permeability, fluid residence times, and mineral reactivity. Moreover, this initial 16S rRNA gene sequence data are just an initial perspective within the broader efforts to fully understand feedbacks between microbial activity, aqueous geochemistry and mineralogy. Isolating and culturing the peridotite-hosted organisms will be an important step in understanding their true metabolic activities and how they adapt to the carbon-depleted, hyperalkaline fluid environment. The microorganisms may be utilizing carbonate veins as a carbon source, leading to mineral dissolution and potential methane production. Additionally, microbial consumption of hydrogen from water/rock reactions may increase the rate of hydrogen-producing reactions. Furthermore, in-situ microbes may be generating distinct organic, mineral and/or isotopic biosignatures in serpentinizing environments that can be used to identify microbial activity remotely.

Examining the functional activity of microbial life in the subsurface will be important to fully understand the coupling between the water/rock reactions, production of reduced gases, and changes in aquifer chemistry and hydrology. A next step for studying the coupling between the hydrological and geochemical processes and the distribution and activity of subsurface microbial life will be to focus on process rate measurements of in-situ hydrogen generation and consumption, pathways of C assimilation and uptake, and

rates of methanogenesis, sulfate reduction, and nitrate reduction. Intensive culturing of peridotite-adapted microorganisms in the laboratory will also be necessary to elucidate the operative metabolic pathways. All of these efforts will be greatly facilitated by the International Continental Drilling Program (ICDP) project in Oman (https://www.ldeo.columbia.edu/gpg/projects/icdp-workshop-oman-drilling-project). The results from this scientific endeavor will give further insight into predicted mineralogy, microbiology, gas generation and C cycling of planetary systems undergoing active alteration of peridotite in the shallow subsurface.

Acknowledgements

The authors would like to thank Tori Hoehler and Mike Kubo (NASA Ames) for providing exploratory organic acid analyses; Said Nasser Al-Habsi and Salim Mohammed Al Khanbashi of the Ministry of Regional Municipalities and Water Resources Sultanate of Oman for granting access to well fluids and drill cuttings; Amelia Paukert for providing supporting information and samples. We would also like to thank numerous colleagues at the University of Colorado at Boulder: Julien Allaz and the electron microprobe lab, the Raman lab, Fred Luiszer at the Laboratory for Environmental and Geological Studies, the Barger lab with their total organic carbon analyzer, the Fierer lab for their sequencing help, Lisa Mayhew for valued discussions and Kaitlin Rempfert for help collecting samples in 2015. Raman imaging and spectroscopy was conducted at the Raman Microspectroscopy Laboratory at the Department of Geological Sciences, University of Colorado-Boulder. Use of the Stanford Synchrotron Radiation Lightsource, SLAC National Accelerator Laboratory, is supported by the U.S. Department of Energy, Office of Science, Office of Basic Energy Sciences under Contract No. DE-AC02-76SF00515, in collaboration with staff scientists Sam Webb, Courtney Krest, and Ryan Davis. This research was funded by the Department of Energy (DE-SC0006886), the NASA Astrobiology Institute (Cooperative Agreement NNA15BB02A), Alfred P. Sloan Foundation Grant 2014-3-01, and NSFEAR-1049905.

Appendix A. Supplementary data

Download Word document (48KB)Help with docx files

Supplementary data. This document file contains Supplementary Tables S1–S3.

References

Abrajano et al., 1990

T.A. Abrajano, N.C. Sturchio, B.M. Kennedy, G.L. Lyon, K. Muehlenbachs, J.K. Bohlke**Geochemistry of reduced gas related to serpentinization of the Zambales ophiolite, Philippines**

Appl. Geochem., 5 (1990), pp. 625-630
ArticleDownload PDFView Record in Scopus
Anderson et al., 1998
R.T. Anderson, F.H. Chapelle, D.R. Lovley**Evidence against hydrogen-based microbial ecosystems in basalt aquifers**
Science, 281 (1998), pp. 976-977
CrossRefView Record in Scopus
Andreani et al., 2013
M. Andreani, M. Muñoz, C. Marcaillou, A. Delacour**µXANES study of iron redox state in serpentine during oceanic serpentinization**
Lithos, 178 (2013), pp. 70-83
ArticleDownload PDFView Record in Scopus
Bach et al., 2006
W. Bach, H. Paulick, C.J. Garrido, B. Ildefonse, W.P. Meurer, S.E. Humphris**Unraveling the sequence of serpentinization reactions: petrography, mineral chemistry, and petrophysics of serpentinites from MAR 15°N (ODP Leg 209, Site 1274)**
Geophys. Res. Lett., 33 (2006)
Available at: http://doi.wiley.com/10.1029/2006GL025681 (accessed 19.05.15)
Balch et al., 1979
W.E. Balch, G.E. Fox, L.J. Magrum, C.R. Woese, R.S. Wolfe**Methanogens: reevaluation of a unique biological group**
Microbiol. Rev., 43 (1979), pp. 260-296
View Record in Scopus
Barberán et al., 2015
A. Barberán, J. Ladau, J.W. Leff, K.S. Pollard, H.L. Menninger, R.R. Dunn, N. Fierer**Continental-scale distributions of dust-associated bacteria and fungi**
Proc. Natl. Acad. Sci. U.S.A., 112 (2015), pp. 5756-5761
CrossRefView Record in Scopus
Barnes and O'Neil, 1969
I. Barnes, J.R. O'Neil**The relationship between fluids in some fresh alpine-type ultramafics and possible modern serpentinization, western United States**
Geol. Soc. Am. Bull., 80 (1969), pp. 1947-1960
CrossRefView Record in Scopus
Barnes et al., 1967
I. Barnes, V.C. LaMarche, G. Himmelberg**Geochemical evidence of present-day serpentinization**
Science, 156 (1967), pp. 830-832
View Record in Scopus
Barnes et al., 1978

I. Barnes, J.R. O'Neil, J.J. Trescases**Present day serpentinization in New Caledonia, Oman and Yugoslavia**
Geochim. Cosmochim. Acta, 42 (1978), pp. 144-145
ArticleDownload PDFView Record in Scopus

Bottinga, 1969

Y. Bottinga**Calculated fractionation factors for carbon and hydrogen isotope exchange in the system calcite-carbon dioxide-graphite-methane-hydrogen-water vapor**
Geochim. Cosmochim. Acta, 33 (1969), pp. 49-64
ArticleDownload PDFView Record in Scopus

Boudier et al., 2010

F. Boudier, A. Baronnet, D. Mainprice**Serpentine mineral replacements of natural olivine and their seismic implications: oceanic lizardite versus subduction-related antigorite**
J. Petrol., 51 (2010), pp. 495-512
CrossRefView Record in Scopus

Bowers et al., 2013

R.M. Bowers, N. Clements, J.B. Emerson, C. Wiedinmyer, M.P. Hannigan, N. Fierer**Seasonal variability in bacterial and fungal diversity of the near-surface atmosphere**
Environ. Sci. Technol., 47 (2013), pp. 12097-12106
CrossRefView Record in Scopus

Brazelton et al., 2012

W.J. Brazelton, B. Nelson, M.O. Schrenk**Metagenomic evidence for H2 oxidation and H2 production by serpentinite-hosted subsurface microbial communities**
Front. Microbiol., 2 (2012)
Available at: <http://www.frontiersin.org/Journal/10.3389/fmicb.2011.00268/full> (accessed 30.01.14)

Brazelton-

et al., 2013

W.J. Brazelton, P.L. Morrill, N. Szponar, M.O. Schrenk**Bacterial communities associated with subsurface geochemical processes in continental serpentinite springs**
Appl. Environ. Microbiol., 79 (2013), pp. 3906-3916
CrossRefView Record in Scopus

Bruni et al., 2002

J. Bruni, M. Canepa, G. Chiodini, R. Cioni, F. Cipolli, A. Longinelli, L. Marini, G. Ottonello, Zuccolini M. Vetuschi**Irreversible water–rock mass transfer accompanying the generation of the neutral, Mg–HCO_3 and high-pH, Ca–OH spring waters of the Genova province, Italy**
Appl. Geochem., 17 (2002), pp. 455-474
ArticleDownload PDFView Record in Scopus

Butler and Banerjee, 1975

R. Butler, S. Banerjee**Theoretical single-domain grain size range m magnetite and titanomagnetite**
J. Geophys. Res. (1975), pp. 4049-4058
CrossRef

Cardace and Ho 2009

D. Cardace, T.M. Hoehler**Serpentinizing fluids craft microbial habitat**
Northeast. Nat., 16 (2009), pp. 272-284
CrossRefView Record in Scopus

Cardace et al., 2

D. Cardace, D.R. Meyer-Dombard, K.M. Woycheese, C.A. Arcilla**Feasible metabolisms in high pH springs of the Philippines**
Front. Microbiol., 6 (2015)

Available at: <http://journal.frontiersin.org/Article/10.3389/fmicb.2015.00010/abstract> (accessed 21.05.15)

Chapelle et al., 2

F.H. Chapelle, K. O'Neill, P.M. Bradley, B.A. Methé, S.A. Ciufo, L.L. Knobel, D.R. Lovley**A hydrogen-based subsurface microbial community dominated by methanogens**
Nature, 415 (2002), pp. 312-315
CrossRefView Record in Scopus

Chavagnac et al

V. Chavagnac, G. Ceuleneer, C. Monnin, B. Lansac, G. Hoareau, C. Boulart**Mineralogical assemblages forming at hyperalkaline warm springs hosted on ultramafic rocks: a case study of Oman and Ligurian ophiolites**
Geochem. Geophys. Geosyst., 14 (2013), pp. 2474-2495
CrossRefView Record in Scopus

Chavagnac et al

V. Chavagnac, C. Monnin, G. Ceuleneer, C. Boulart, G. Hoareau**Characterization of hyperalkaline fluids produced by low-temperature serpentinization of mantle peridotites in the Oman and Ligurian ophiolites**
Geochem. Geophys. Geosyst., 14 (2013), pp. 2496-2522
CrossRefView Record in Scopus

Clark and Fontes

I.D. Clark, J.-C. Fontes**Paleoclimatic reconstruction in northern Oman based on carbonates from hyperalkaline groundwaters**
Quat. Res., 33 (1990), pp. 320-336
ArticleDownload PDFCrossRefView Record in Scopus

Coleman, 1981

R.G. Coleman**Tectonic setting for ophiolite obduction in Oman**
J. Geophys. Res. Solid Earth, 86 (1981), pp. 2497-2508
CrossRefView Record in Scopus

Dewandel et al.,

B. Dewandel, P. Lachassagne, F. Boudier, S. Al-Hattali, B. Ladouche, J.-L. Pinault, Z. Al-Suleimani**A conceptual hydrogeological model of ophiolite hard-rock aquifers in Oman based on a multiscale and a multidisciplinary approach**
Hydrogeol. J., 13 (2005), pp. 708-726
CrossRefView Record in Scopus

Downs, 2006

R.T. Downs**The RRUFF project: an integrated study of the chemistry, crystallography, Raman and infrared spectroscopy of minerals**
Program and Abstracts of the 19th General Meeting of the International Mineralogical Association in Kobe, Japan (2006), pp. O03-13

View Record in Scopus

Dunlop, 1973

D.J. Dunlop**Superparamagnetic and single-domain threshold sizes in magnetite**
J. Geophys. Res., 78 (1973), pp. 1780-1793
CrossRefView Record in Scopus

Edgar, 2013

R.C. Edgar**UPARSE: highly accurate OTU sequences from microbial amplicon reads**
Nat. Methods, 10 (2013), pp. 996-998
CrossRefView Record in Scopus

Emerson et al., 2

J.B. Emerson, P.B. Keady, T.E. Brewer, N. Clements, E.E. Morgan, J. Awerbuch, S.L.Miller, N. Fierer**Impacts of flood damage on airborne bacteria and fungi in homes after the 2013 Colorado front range flood**
Environ. Sci. Technol., 49 (2015), pp. 2675-2684
CrossRefView Record in Scopus

Etiope and Sherw

G. Etiope, B. Sherwood Lollar**Abiotic methane on earth**
Rev. Geophys., 51 (2013), pp. 276-299
CrossRefView Record in Scopus

Etiope et al., 201

G. Etiope, M. Schoell, H. Hosgörmez**Abiotic methane flux from the Chimaera seep and Tekirova ophiolites (Turkey): understanding gas exhalation from low temperature serpentinization and implications for Mars**
Earth Planet. Sci. Lett., 310 (2011), pp. 96-104
ArticleDownload PDFView Record in Scopus

Etiope et al., 201

G. Etiope, B.L. Ehlmann, M. Schoell**Low temperature production and exhalation of methane from serpentinized rocks on Earth: a potential analog for methane production on Mars**
Icarus, 224 (2013), pp. 276-285
ArticleDownload PDFView Record in Scopus

Evans, 2004

B.W. Evans**The serpentinite multisystem revisited: chrysotile is metastable**
Int. Geol. Rev., 46 (2004), pp. 479-506
CrossRefView Record in Scopus

Evans, 2010

B.W. Evans**Lizardite versus antigorite serpentinite: magnetite, hydrogen, and life (?)**
Geology, 38 (2010), pp. 879-882
CrossRefView Record in Scopus

Evans et al., 200

B.W. Evans, S.M. Kuehner, A. Chopelas**Magnetite-free, yellow lizardite serpentinization of olivine websterite, Canyon Mountain complex, N.E. Oregon**
Am. Mineral., 94 (2009), pp. 1731-1734
CrossRefView Record in Scopus

Frost, 1985

B.R. Frost**On the stability of sulfides, oxides, and native metals in serpentinite**
J. Petrol., 26 (1985), pp. 31-63
CrossRefView Record in Scopus

Frost and Beard,

B.R. Frost, J.S. Beard**On silica activity and serpentinization**
J. Petrol., 48 (2007), pp. 1351-1368
CrossRef

Groppo et al., 20

C. Groppo, C. Rinaudo, S. Cairo, D. Gastaldi, R. Compagnoni**Micro-Raman spectroscopy for a quick and reliable identification of serpentine minerals from ultramafics**
Eur. J. Mineral., 18 (2006), pp. 319-329
CrossRefView Record in Scopus

Hanghøj et al., 2

K. Hanghøj, P.B. Kelemen, D. Hassler, M. Godard**Composition and genesis of depleted mantle peridotites from the Wadi Tayin Massif, Oman Ophiolite; major and trace element geochemistry, and Os isotope and PGE systematics**
J. Petrol., 51 (2010), pp. 201-227
CrossRefView Record in Scopus

Haouari et al., 20

O. Haouari, M.-L. Fardeau, J.-L. Cayol, G. Fauque, C. Casiot, F. Elbaz-Poulichet, M. Hamdi, B. Ollivier***Thermodesulfovibrio hydrogeniphilus* sp. nov., a new thermophilic sulphate-reducing bacterium isolated from a Tunisian hot spring**
Syst. Appl. Microbiol., 31 (2008), pp. 38-42
ArticleDownload PDFView Record in Scopus

Haroon et al., 20

M.F. Haroon, S. Hu, Y. Shi, M. Imelfort, J. Keller, P. Hugenholtz, Z. Yuan, G.W. Tyson**Anaerobic oxidation of methane coupled to nitrate reduction in a novel archaeal lineage**
Nature, 500 (2013), pp. 567-570
CrossRefView Record in Scopus

Hicks et al., 201

D.B. Hicks, J. Liu, M. Fujisawa, T.A. Krulwich**F1F0-ATP synthases of alkaliphilic bacteria: lessons from their adaptations**
Biochim. Biophys. Acta BBA – Bioenergetics, 1797 (2010), pp. 1362-1377
ArticleDownload PDFView Record in Scopus

Hoehler et al., 19

T.M. Hoehler, M.J. Alperin, D.B. Albert, C.S. Martens**Field and laboratory studies of methane oxidation in an anoxic marine sediment: evidence for a methanogen-sulfate reducer consortium**

Glob. Biogeochem. Cycles, 8 (1994), pp. 451-463

CrossRefView Record in Scopus

Horibe and Craig

Y. Horibe, H. Craig**DH fractionation in the system methane-hydrogen-water**

Geochim. Cosmochim. Acta, 59 (1995), pp. 5209-5217

ArticleDownload PDFView Record in Scopus

Horita and Bernd

J. Horita, M.E. Berndt**Abiogenic methane formation and isotopic fractionation under hydrothermal conditions**

Science, 285 (1999), pp. 1055-1057

CrossRefView Record in Scopus

Hug et al., 2013

L.A. Hug, C.J. Castelle, K.C. Wrighton, B.C. Thomas, I. Sharon, K.R. Frischkorn, K.H. Williams, S .G. Tringe, J.F. Banfield**Community genomic analyses constrain the distribution of metabolic traits across the Chloroflexi phylum and indicate roles in sediment carbon cycling**

Microbiome, 1 (2013), p. 22

CrossRef

Jacquemin et al.

M. Jacquemin, A. Beuls, P. Ruiz**Catalytic production of methane from CO_2 and H_2 at low temperature: insight on the reaction mechanism**

Catal. Today, 157 (2010), pp. 462-466

ArticleDownload PDFView Record in Scopus

Joye et al., 2004

S.B. Joye, A. Boetius, B.N. Orcutt, J.P. Montoya, H.N. Schulz, M.J. Erickson, S.K. Lugo**The anaerobic oxidation of methane and sulfate reduction in sediments from Gulf of Mexico cold seeps**

Chem. Geol., 205 (2004), pp. 219-238

ArticleDownload PDFView Record in Scopus

Kelemen and Hirth, 2012

P.B. Kelemen, G. Hirth**Reaction-driven cracking during retrograde metamorphism: olivine hydration and carbonation**

Earth Planet. Sci. Lett., 345–348 (2012), pp. 81-89

ArticleDownload PDFView Record in Scopus

Kelemen and Matter, 2008

P.B. Kelemen, J. Matter**In situ carbonation of peridotite for CO_2 storage**
Proc. Natl. Acad. Sci. U.S.A., 105 (2008), pp. 17295-17300
CrossRefView Record in Scopus

Kelemen et al., 2011
P.B. Kelemen, J. Matter, E.E. Streit, J.F. Rudge, W.B. Curry, J. Blusztajn**Rates and mechanisms of mineral carbonation in peridotite: natural processes and recipes for enhanced, in situ CO_2 capture and storage**
Annu. Rev. Earth Planet. Sci., 39 (2011), pp. 545-576
CrossRefView Record in Scopus

Klein et al., 2009
F. Klein, W. Bach, N. Jöns, T. McCollom, B. Moskowitz, T. Berquó**Iron partitioning and hydrogen generation during serpentinization of abyssal peridotites from 15°N on the Mid-Atlantic Ridge**
Geochim. Cosmochim. Acta, 73 (2009), pp. 6868-6893
ArticleDownload PDFView Record in Scopus

Klein et al., 2013a
F. Klein, W. Bach, S.E. Humphris, W.-A. Kahl, N. Jons, B. Moskowitz, T.S. Berquo**Magnetite in seafloor serpentinite–some like it hot**
Geology, 42 (2013), pp. 135-138
View Record in Scopus

Klein et al., 2013b
F. Klein, W. Bach, T.M. McCollom**Compositional controls on hydrogen generation during serpentinization of ultramafic rocks**
Lithos, 178 (2013), pp. 55-69
ArticleDownload PDFView Record in Scopus

Klein et al., 2015
F. Klein, S.E. Humphris, W. Guo, F. Schubotz, E.M. Schwarzenbach, W.D. Orsi**Fluid mixing and the deep biosphere of a fossil Lost City-type hydrothermal system at the Iberia Margin**
Proc. Natl. Acad. Sci. U.S.A. (2015), Article 201504674

Kumar and Saravanan, 2011
M.R. Kumar, V.S. Saravanan**Candidate OP phyla: importance, ecology and cultivation prospects**
Indian J. Microbiol., 50 (2011), pp. 474-477
CrossRefView Record in Scopus

Lafay et al., 2012
R. Lafay, G. Montes-Hernandez, E. Janots, R. Chiriac, N. Findling, F. Toche**Mineral replacement rate of olivine by chrysotile and brucite under high alkaline conditions**
J. Cryst. Growth, 347 (2012), pp. 62-72
ArticleDownload PDFView Record in Scopus

Laier and Nytoft, 2012

T. Laier, H.P. Nytoft**Bitumen biomarkers in the mid-proterozoic Ilímaussaq intrusion, Southwest Greenland – a challenge to the mantle gas theory**

Mar. Pet. Geol., 30 (2012), pp. 50-65

ArticleDownload PDFView Record in Scopus

Lang et al., 2010

S.Q. Lang, D.A. Butterfield, M. Schulte, D.S. Kelley, M.D. Lilley**Elevated concentrations of formate, acetate and dissolved organic carbon found at the Lost City hydrothermal field**

Geochim. Cosmochim. Acta, 74 (2010), pp. 941-952

ArticleDownload PDFView Record in Scopus

Lorand, 1987

J. Lorand**A new occurrence of native iron in a serpentinized mantle peridotite - Maqsad, Sumail Massif, Semail Ophiolite (Southern Oman)**

Comptes Rendus Acad. Sci, Ii 304 (1987), pp. 703-706

View Record in Scopus

Madigan, 2012

M.T. Madigan**Brock Biology of Microorganisms**

Benjamin Cummings, San Francisco (2012)

Malvoisin et al., 2012

B. Malvoisin, J. Carlut, F. Brunet**Serpentinization of oceanic peridotites: 1. A high-sensitivity method to monitor magnetite production in hydrothermal experiments**

J. Geophys. Res. Solid Earth, 117 (2012), Article B01104

Marcaillou et al., 2011

C. Marcaillou, M. Muñoz, O. Vidal, T. Parra, M. Harfouche**Mineralogical evidence for H_2 degassing during serpentinization at 300 °C/300 bar**

Earth Planet. Sci. Lett., 303 (2011), pp. 281-290

ArticleDownload PDFView Record in Scopus

Mayhew et al., 2011

L.E. Mayhew, S.M. Webb, A.S. Templeton**Microscale imaging and identification of Fe speciation and distribution during fluid-mineral reactions under highly reducing conditions**

Environ. Sci. Technol., 45 (2011), pp. 4468-4474

CrossRefView Record in Scopus

Mayhew et al., 2013

L.E. Mayhew, E.T. Ellison, T.M. McCollom, T.P. Trainor, A.S. Templeton**Hydrogen generation from low-temperature water–rock reactions**

Nat. Geosci., 6 (2013), pp. 478-484

CrossRefView Record in Scopus

McCollom and Bach, 2009

T.M. McCollom, W. Bach**Thermodynamic constraints on hydrogen generation during serpentinization of ultramafic rocks**
Geochim. Cosmochim. Acta, 73 (2009), pp. 856-875
ArticleDownload PDFView Record in Scopus

McCollom and Seewald, 2001
T.M. McCollom, J.S. Seewald**A reassessment of the potential for reduction of dissolved CO_2 to hydrocarbons during serpentinization of olivine**
Geochim. Cosmochim. Acta, 65 (2001), pp. 3769-3778
ArticleDownload PDFView Record in Scopus

McDonald et al., 2012
D. McDonald, M.N. Price, J. Goodrich, E.P. Nawrocki, T.Z. DeSantis, A. Probst, G.L.Andersen, R. Knight, P. Hugenholtz**An improved Greengenes taxonomy with explicit ranks for ecological and evolutionary analyses of bacteria and archaea**
ISME J., 6 (2012), pp. 610-618
CrossRefView Record in Scopus

Ménez et al., 2012
B. Ménez, V. Pasini, D. Brunelli**Life in the hydrated suboceanic mantle**
Nat. Geosci., 5 (2012), pp. 133-137
CrossRefView Record in Scopus

Mervine et al., 2014
E.M. Mervine, S.E. Humphris, K.W.W. Sims, P.B. Kelemen, W.J. Jenkins**Carbonation rates of peridotite in the Samail Ophiolite, Sultanate of Oman, constrained through 14C dating and stable isotopes**
Geochim. Cosmochim. Acta, 126 (2014), pp. 371-397
ArticleDownload PDFView Record in Scopus

Meyer-Dombard et al., 2015
D.R. Meyer-Dombard, K.M. Woycheese, E.N. Yargıçoğlu, D. Cardace, E.L. Shock, Y. Güleçal-Pektas, M. Temel**High pH microbial ecosystems in a newly discovered, ephemeral, serpentinizing fluid seep at Yanartaş (Chimera), Turkey**
Front. Microbiol., 5 (2015)
Available at: <http://journal.frontiersin.org/article/10.3389/fmicb.2014.00723/abstract> (accessed 07.03.15)

Moody, 1976
J.B. Moody**Serpentinization: a review**
Lithos, 9 (1976), pp. 125-138
ArticleDownload PDFView Record in Scopus

Morrill et al., 2013

P.L. Morrill, J.G. Kuenen, O.J. Johnson, S. Suzuki, A. Rietze, A.L. Sessions, M.L. Fogel, K.H.Nealson**Geochemistry and geobiology of a present-day serpentinization site in California: the Cedars**
Geochim. Cosmochim. Acta, 109 (2013), pp. 222-240
ArticleDownload PDFView Record in Scopus

Mulkidjanian et al., 2008
A.Y. Mulkidjanian, P. Dibrov, M.Y. Galperin**The past and present of sodium energetics: may the sodium-motive force be with you**
Biochim. Biophys. Acta BBA – Bioenergetics, 1777 (2008), pp. 985-992
ArticleDownload PDFView Record in Scopus

Muñoz et al., 2013
M. Muñoz, O. Vidal, C. Marcaillou, S. Pascarelli, O. Mathon, F. Farges**Iron oxidation state in phyllosilicate single crystals using Fe-K pre-edge and XANES spectroscopy: effects of the linear polarization of the synchrotron X-ray beam**
Am. Mineral., 98 (2013), pp. 1187-1197
CrossRefView Record in Scopus

Neal and Stanger, 1983
C. Neal, G. Stanger**Hydrogen generation from mantle source rocks in Oman**
Earth Planet. Sci. Lett., 66 (1983), pp. 315-320
ArticleDownload PDFView Record in Scopus

Neal and Stanger, 1984
C. Neal, G. Stanger**Calcium and magnesium hydroxide precipitation from alkaline groundwaters in Oman, and their significance to the process of serpentinization**
Mineral. Mag., 48 (1984), pp. 237-241
View Record in Scopus

Neal and Stanger, 1985
C. Neal, G. Stanger**Past and present serpentinisation of ultramafic rocks; an example from the Semail ophiolite Nappe of Northern Oman**
J.I. Drever (Ed.), The Chemistry of Weathering. Nato ASI Series, Springer, Netherlands (1985), pp. 249-275
Available at: <http://link.springer.com/chapter/10.1007/978-94-009-5333-8_15> (accessed 17.06.15)
CrossRefView Record in Scopus

Nealson et al., 2005
K.H. Nealson, F. Inagaki, K. Takai**Hydrogen-driven subsurface lithoautotrophic microbial ecosystems (SLiMEs): do they exist and why should we care?**
Trends Microbiol., 13 (2005), pp. 405-410
ArticleDownload PDFView Record in Scopus

Neubeck et al., 2011

A. Neubeck, N.T. Duc, D. Bastviken, P. Crill, N.G. Holm**Formation of H_2 and CH_4 by weathering of olivine at temperatures between 30 and 70 °C**
Geochem. Trans., 12 (2011), p. 6
CrossRef

Nielsen and Nielsen, 1998
J.L. Nielsen, P.H. Nielsen**Microbial nitrate-dependent oxidation of ferrous iron in activated sludge**
Environ. Sci. Technol., 32 (1998), pp. 3556-3561
CrossRefView Record in Scopus

Okland et al., 2012
I. Okland, S. Huang, H. Dahle, I.H. Thorseth, R.B. Pedersen**Low temperature alteration of serpentinized ultramafic rock and implications for microbial life**
Chem. Geol., 318–319 (2012), pp. 75-87
ArticleDownload PDFView Record in Scopus

Pasini et al., 2013
V. Pasini, D. Brunelli, P. Dumas, C. Sandt, J. Frederick, K. Benzerara, S. Bernard, B. Ménez**Low temperature hydrothermal oil and associated biological precursors in serpentinites from Mid-Ocean Ridge**
Lithos, 178 (2013), pp. 84-95
ArticleDownload PDFView Record in Scopus

Paukert et al., 2012
A.N. Paukert, J.M. Matter, P.B. Kelemen, E.L. Shock, J.R. Havig**Reaction path modeling of enhanced in situ CO_2 mineralization for carbon sequestration in the peridotite of the Samail Ophiolite, Sultanate of Oman**
Chem. Geol., 330–331 (2012), pp. 86-100
ArticleDownload PDFView Record in Scopus

Petriglieri et al., 2015
J.R. Petriglieri, E. Salvioli-Mariani, L. Mantovani, M. Tribaudino, P.P. Lottici, C. Laporte-Magoni, D. Bersani**Micro-Raman mapping of the polymorphs of serpentine**
J. Raman Spectrosc. (2015)
n/a–n/a

Postec et al., 2015
A. Postec, M. Quéméneur, M. Bes, N. Mei, F. Benaïssa, C. Payri, B. Pelletier, C. Monnin, L.Guentas-Dombrowsky, B. Ollivier, E. Gérard, C. Pisapia, M. Gérard, B. Ménez, G. Erauso**Microbial diversity in a submarine carbonate edifice from the serpentinizing hydrothermal system of the Prony Bay (New Caledonia) over a 6-year period**
Front. Microbiol., 6 (2015)
Available at: <http://www.ncbi.nlm.nih.gov/pmc/articles/PMC4551099/> (accessed 20.11.15)

Proskurowski et al., 2006

G. Proskurowski, M.D. Lilley, D.S. Kelley, E.J. Olson**Low temperature volatile production at the Lost City Hydrothermal Field, evidence from a hydrogen stable isotope geothermometer**
Chem. Geol., 229 (2006), pp. 331-343
ArticleDownload PDFView Record in Scopus

R Development Core Team, 2008
R Development Core Team**R: A Language and Environment for Statistical Computing**
R Foundation for Statistical Computing, Vienna, Austria (2008)
Available at: <http://www.R-project.org>

Ravaut et al., 1997
P. Ravaut, R. Bayer, R. Hassani, D. Rousset, A.A. Yahya'ey**Structure and evolution of the northern Oman margin: gravity and seismic constraints over the Zagros-Makran-Oman collision zone**
Tectonophysics, 279 (1997), pp. 253-280
ArticleDownload PDFView Record in Scopus

Rinaudo et al., 2003
C. Rinaudo, D. Gastaldi, E. Belluso**Characterization of chrysotile, antigorite and lizardite by Ft-Raman spectroscopy**
Can. Mineral., 41 (2003), pp. 883-890
CrossRefView Record in Scopus

Schrenk et al., 2013
M.O. Schrenk, W.J. Brazelton, S.Q. Lang**Serpentinization, carbon, and deep life**
Rev. Mineral. Geochem., 75 (2013), pp. 575-606
CrossRefView Record in Scopus

Sherwood Lollar et al., 1993
B. Sherwood Lollar, S.K. Frape, S.M. Weise, P. Fritz, S.A. Macko, J.A. Welhan**Abiogenic methanogenesis in crystalline rocks**
Geochim. Cosmochim. Acta, 57 (1993), pp. 5087-5097
ArticleDownload PDFView Record in Scopus

Sleep et al., 2004
N.H. Sleep, A. Meibom, T. Fridriksson, R.G. Coleman, D.K. Bird**H_2-rich fluids from serpentinization: geochemical and biotic implications**
Proc. Natl. Acad. Sci. U.S.A., 101 (2004), pp. 12818-12823
CrossRefView Record in Scopus

Stanger, 1986
G. Stanger**The Hydrogeology of the Oman Mountains**
Open University London (1986)

Stevens and McKinley, 1995
T.O. Stevens, J.P. McKinley**Lithoautotrophic microbial ecosystems in deep basalt aquifers**

Science, 270 (1995), pp. 450-455
View Record in Scopus

Stevens and McKinley, 2000

T.O. Stevens, J.P. McKinley**Abiotic controls on H_2 production from Basalt−Water reactions and implications for aquifer biogeochemistry**
Environ. Sci. Technol., 34 (2000), pp. 826-831
CrossRefView Record in Scopus

Streit et al., 2012

E. Streit, P. Kelemen, J. Eiler**Coexisting serpentine and quartz from carbonate-bearing serpentinized peridotite in the Samail Ophiolite, Oman**
Contrib. Mineral. Petrol., 164 (2012), pp. 821-837
CrossRefView Record in Scopus

Suzuki et al., 2013

S. Suzuki, S. Ishii, A. Wu, A. Cheung, A. Tenney, G. Wanger, J.G. Kuenen, K.H. Nealson**Microbial diversity in The Cedars, an ultrabasic, ultrareducing, and low salinity serpentinizing ecosystem**
Proc. Natl. Acad. Sci. U.S.A., 110 (2013), pp. 15336-15341
CrossRefView Record in Scopus

Suzuki et al., 2014

S. Suzuki, J.G. Kuenen, K. Schipper, S. van der Velde, S. Ishii, A. Wu, D.Y. Sorokin, A.Tenney, X. Meng, P.L. Morrill, Y. Kamagata, G. Muyzer, K.H. Nealson**Physiological and genomic features of highly alkaliphilic hydrogen-utilizing Betaproteobacteria from a continental serpentinizing site**
Nat. Commun., 5 (2014)
Available at: <http://www.nature.com/ncomms/2014/140521/ncomms4900/full/ncomms4900.html> (accessed 19.11.14)

Takami et al., 2012

H. Takami, H. Noguchi, Y. Takaki, I. Uchiyama, A. Toyoda, S. Nishi, G.-J. Chee, W. Arai, T.Nunoura, T. Itoh, M. Hattori, K. Takai**A deeply branching thermophilic bacterium with an ancient acetyl-CoA pathway dominates a subsurface ecosystem**
PLoS ONE, 7 (2012), Article e30559
CrossRef

Tauxe et al., 2014

L. Tauxe, S.K. Banerjee, R.F. Butler, R. van der Voo**Essentials of Paleomagnetism**
(3rd Web ed.) (2014)

Templeton et al., 2006

A.S. Templeton, K.-H. Chu, L. Alvarez-Cohen, M.E. Conrad**Variable carbon isotope fractionation expressed by aerobic CH_4-oxidizing bacteria**

Geochim. Cosmochim. Acta, 70 (2006), pp. 1739-1752
ArticleDownload PDFView Record in Scopus

Tindall et al., 2010

B.J. Tindall, J. Sikorski, S. Lucas, E. Goltsman, A. Copeland, T. Glavina Del Rio, M. Nolan, H.Tice, J.-F. Cheng, C. Han, S. Pitluck, K. Liolios, N. Ivanova, K. Mavromatis, G. Ovchinnikova, A. Pati, R.Fähnrich, L. Goodwin, A. Chen, K. Palaniappan, M. Land, L. Hauser, Y.-J. Chang, C.D. Jeffries, M.Rohde, M. Göker, T. Woyke, J. Bristow, J.A. Eisen, V. Markowitz, P. Hugenholtz, N.C. Kyrpides, H.-P.Klenk, A. Lapidus**Complete genome sequence of Meiothermus ruber type strain (21T)**
Stand. Genomic Sci., 3 (2010), pp. 26-36
CrossRefView Record in Scopus

Wang et al., 2007

Q. Wang, G.M. Garrity, J.M. Tiedje, J.R. Cole**Naive Bayesian classifier for rapid assignment of rRNA sequences into the new bacterial taxonomy**
Appl. Environ. Microbiol., 73 (2007), pp. 5261-5267
CrossRefView Record in Scopus

Weyhenmeyer, 2000

C. Weyhenmeyer**Origin and evolution of groundwaters in the alluvial aquifer of the Eastern Batinah Coastal Plain, Sultanate of Oman**
Ph.D. thesis
Univ. Bern Switz (2000)

Whiticar, 1990

M.J. Whiticar**A geochemial perspective of natural gas and atmospheric methane**

Org. Geochem., 16 (1990), pp. 531-547
ArticleDownload PDFView Record in Scopus

Whiticar, 1999

M.J. Whiticar**Carbon and hydrogen isotope systematics of bacterial formation and oxidation of methane**
Chem. Geol., 161 (1999), pp. 291-314
ArticleDownload PDFView Record in Scopus

Whiticar and Faber, 1986

M.J. Whiticar, E. Faber**Methane oxidation in sediment and water column environments—isotope evidence**
Org. Geochem., 10 (1986), pp. 759-768
ArticleDownload PDFView Record in Scopus

Wilke et al., 200

M. Wilke, F. Farges, P.-E. Petit, G.E. Brown, F. Martin**Oxidation state and coordination of Fe in minerals: An Fe K-XANES spectroscopic study**
Am. Mineral., 86 (2001), pp. 714-730
CrossRefView Record in Scopus

Willems et al., 19

A. Willems, J. Busse, M. Goor, B. Pot, E. Falsen, E. Jantzen, B. Hoste, M. Gillis, K. Kersters, G. A uling, *et al.***Hydrogenophaga, a new genus of hydrogen-oxidizing bacteria that includes Hydrogenophaga flava comb. nov.(formerly Pseudomonas flava), Hydrogenophaga palleronii (formerly Pseudomonas palleronii), Hydrogenophaga pseudoflava (formerly Pseudomonas pseudoflava and “Pseudomonas carboxydoflava”), and Hydrogenophaga taeniospiralis (formerly Pseudomonas taeniospiralis)**
Int. J. Syst. Bacteriol., 39 (1989), pp. 319-333
CrossRefView Record in Scopus

Worm, 1998

H.-U. Worm**On the superparamagnetic—stable single domain transition for magnetite, and frequency dependence of susceptibility**
Geophys. J. Int., 133 (1998), pp. 201-206
CrossRefView Record in Scopus

Woycheese et al

K.M. Woycheese, D.R. Meyer-Dombard, D. Cardace, A.M. Argayosa, C.A. Arcilla**Out of the dark: transitional subsurface-to-surface microbial diversity in a terrestrial serpentinizing seep (Manleluag, Pangasinan, the Philippines)**
Front. Microbiol., 6 (2015)

Available at: <http://journal.frontiersin.org/Article/10.3389/fmicb.2015.00044/abstract> (accessed 21.05.15)